Microinvasion and immunity elicited by disease-attenuated pneumococcal biosynthesis gene mutants

Caroline M. Weight[1*], Gabriele Pollara[1], Modupeh Betts[1], Roberta Ragazzini[2], Elisa Ramos-Sevillano[3], Jesús Reiné[4], Matthew Whelan[1], José Afonso Guerra-Assunção[1], Michael Connor[5], Paola Bonfanti[1,2], Clare Jolly[1], Mahdad Noursadeghi[1], Daniela M. Ferreira[4], Jeremy S. Brown[3], Robert S. Heyderman[1]

[1]Research Department of Infection, Division of Infection and Immunity, UCL London, UK

[2]Francis Crick Institute, London, UK

[3]Department of Respiratory Medicine, UCL, London, UK

[4]Oxford Vaccine Group, University of Oxford, Oxford and Clinical Sciences, Liverpool School of Tropical Medicine, Liverpool, UK

[5]Chromatin and Infection, Institut Pasteur, France

*Current address Biomedical and Life Sciences, Faculty of Health and Medicine, Lancaster University, UK

Corresponding Authors: Dr Caroline M. Weight and Professor Robert S. Heyderman

Email: c.weight@lancaster.ac.uk and r.heyderman@ucl.ac.uk

ABSTRACT

Nasopharyngeal colonisation by *Streptococcus pneumoniae* is characterised epithelial cell adherence, microinvasion and an innate immune response. Here, we explore the hypothesis that pneumococcal virulence has primarily evolved to promote colonisation and transmission, rather than to cause disease. We used a *S. pneumoniae* serotype 6B strain alongside two biosynthesis gene mutants (Δ*proABC* and Δ*fhs*). These mutations did not attenuate pneumococcal microinvasion in either experimental human pneumococcal challenge or *in vitro* in primary and immortalised epithelial cells, but we did observe strain-dependent differences following infection. These included cellular reorganisation, pro-inflammatory epithelial innate responses and caspase 8 activity and, secretion of pneumococcal hydrogen peroxide secretion and pneumolysin activity. Bacterial transcriptomic analysis, under stress conditions, revealed that deletion of these biosynthesis genes had broad, differential effects on pneumococcal virulence and metabolic gene expression, suggestive of compensatory changes that preserve microinvasion. The findings that cellular reorganisation, the innate immune response, and the ability to cause invasive disease are not necessarily interconnected emphasise the outcome of colonisation cannot be fully explained by single or functionally grouped virulence or metabolic factors.

Keywords

Biosynthesis genes/host-pathogen interactions/Innate immunity/*Streptococcus pneumoniae*/respiratory epithelium

Graphical Abstract

S. pneumoniae colonisation is characterised by mucus association, epithelial adherence and microinvasion – where the pneumococcus invades the epithelial barrier without causing disease. Microcolonies form at the epithelial surface and pneumococcal transmigration can occur between epithelial cells. Although mutations in *S. pneumoniae* biosynthesis genes (Δ*proABC* and Δ*fhs*) attenuate disease in a murine model, they do not attenuate microinvasion in either experimental

human pneumococcal challenge (EHPC) or *in vitro* in primary and immortalised epithelial cells. These mutations show strain-dependent effects on both the epithelial and bacterial responses to infection. While not directly co-correlated, factors such as epithelial cellular reorganisation, inflammation and caspase 8 activity alongside pneumococcal metabolic adaptation, virulence factor expression and response to stress are key determinants of the outcome of colonisation in the nasopharyngeal niche.

INTRODUCTION

Adaptation to the host environment is crucial for successful colonisation of the upper respiratory tract (URT) by a range of human pathogens, including bacteria, viruses and fungi. This includes the ability to withstand different ambient temperatures, overcome physical barriers such as mucus, evade epithelial soluble mediators such as antimicrobial peptides, compete with neighbouring polymicrobial communities and compensate for nutrient restriction (Weiser, Ferreira et al., 2018). *Streptococcus pneumoniae* (the pneumococcus) is a common commensal of this URT niche (Weiser et al., 2018). However, translocation of the pneumococcus from the nasopharynx to the lungs, blood or the brain results in life-threatening disease (Weiser et al., 2018). Indeed, among children under five years, *S. pneumoniae* is the leading cause of pneumonia deaths globally (O'Brien, Wolfson et al., 2009).

Using experimental human pneumococcal challenge (EHPC) of healthy volunteers and well-characterised epithelial cell models, we have previously shown that colonisation by *S. pneumoniae* is characterised by epithelial surface microcolony formation and invasion which we have called microinvasion (i.e. invasion of the epithelial barrier without disease) (Weight, Venturini et al., 2019). The pneumococcal capsule is a major virulence determinant, influencing carriage, transmission from person to person, and invasive disease potential (Zafar, Hamaguchi et al., 2017a). Indeed, we have shown that *S. pneumoniae* epithelial microinvasion also varies markedly between strains expressing different capsular serotypes, with a serotype 4 strain invading Detroit 562 nasopharyngeal cell monolayers more readily than serotype 6B and 23F strains, and inducing more marked pro-inflammatory epithelial transcriptomic and cytokine responses (Weight et al., 2019).

We and others have previously proposed that although the epithelial innate immune response that results from pneumococcal colonisation may facilitate clearance, this highly variable pathobiont (>100 serotypes; >600 global pneumococcal sequence clusters (Gladstone, Lo et al., 2019)) tunes the host response to enhance transmission(Weight et al., 2019, Zafar et al., 2017a). In addition to

83 capsule, these processes have been shown to be modulated by a broad array of subcapsular and
84 cytoplasmic virulence factors (Amin-Chowdhury, Collins et al., 2020), and more recently, by bacterial
85 carbohydrate, nucleotide, fatty acid and purine/ pyrimidine metabolism (Echlin, Frank et al., 2020,
86 Hartel, Eylert et al., 2012, Henriques-Normark & Tuomanen, 2013, Kohler, Voss et al., 2016, van
87 Opijnen & Camilli, 2012).

88

89 To explore the hypothesis that pneumococcal virulence has primarily evolved to promote
90 colonisation and subsequent transmission, but not necessarily disease, we have used a unique set
91 of *S. pneumoniae* serotype 6B Δ*proABC* and Δ*fhs* biosynthesis gene mutants developed to induce
92 protective immunity without causing disease (Ramos-Sevillano, Ercoli et al., 2020). *proABC* and *fhs*
93 were chosen as targets through the analysis of previously published transcriptome and transposon
94 mutational screens (Mahdi, Wang et al., 2012, Ogunniyi, Mahdi et al., 2012, van Opijnen & Camilli,
95 2012). The *proABC* operon, consisting of genes predicted to encode a γ-glutamyl phosphate
96 reductase (*proA*), a γ-glutamyl kinase (*proB*) and a pyrroline-5-carboxylate reductase (*proC*), and
97 *fhs* predicted to encode a folate tetrahydrofolate reductase involved in one carbon metabolism
98 pathways have been implicated in metabolic adaptation to growth (Brill, Hoffmann et al., 2011,
99 Crowley, Gutierrez et al., 1997, Ramos-Sevillano E., 2023), and are highly transcribed in mouse
100 models of pneumococcal infection (Crowley et al., 1997, Ramos-Sevillano E., 2023). To further avoid
101 reversion to a disease-causing phenotype during EHPC, these mutants also contain a deletion of
102 *piaA* which encodes the lipoprotein component of the dominant pneumococcal iron uptake ABC
103 transporter (Brown, Gilliland et al., 2001, Hill, Mitsi et al., 2023). We have previously shown that in a
104 murine model, when compared to the *S. pneumoniae* serotype 6B wild-type parent strain (WT,
105 BHN418), the Δ*proABC/piaA* and Δ*fhs/piaA* mutants colonise the nasopharynx as effectively.
106 However, despite expressing the same capsule as the wild type 6B strain, neither the Δ*proABC/piaA*
107 and Δ*fhs/piaA* 6B strains causes invasive disease (Ramos-Sevillano et al., 2020) (17). We have
108 subsequently shown that this attenuated phenotype is at least in part due to impaired growth in
109 serum and is associated with increased oxidative stress and altered lipid profiles (17). In EHPC, we
110 have also shown that both Δ*proABC/piaA* and Δ*fhs/piaA* retain the ability to colonise the human host,

111 and can induce IgG-mediated immunity (Hill H, 2023). Therefore, these otherwise isogenic strains
112 allow us to compare the pneumococcal-epithelial interactions of disease-causing and non-disease-
113 causing phenotypes, while avoiding the confounding of differences in capsular serotype.

114

115 Here, we reveal that although the *S. pneumoniae* Δ*proABC/piaA* and Δ*fhs/piaA* metabolic function
116 mutations result in disease attenuation, the ability of the mutant strains to colonise and cause
117 microinvasion in both EHPC and *in vitro* epithelial infection models is preserved. Crucially, we also
118 show that despite similar patterns of epithelial cellular engagement, disruption of these key
119 pneumococcal metabolic pathways has differential effects on cellular reorganisation and innate
120 responses, which we propose influences niche adaptation during colonisation.

121

122 **RESULTS**

123

124 ***S. pneumoniae* 6B with Δ*proABC* or Δ*fhs* mutants colonise in EHPC with evidence of epithelial**
125 **microinvasion**

126 We have defined microinvasion as the process by which *S. pneumoniae* invades the mucosal
127 epithelium, inducing an innate immune response, without necessarily causing disease (Fig 1A).
128 Nasal curette samples from EHPC healthy volunteers inoculated with the *S. pneumoniae* serotype
129 6B WT or isogenic mutant strains (Δ*proABC/piaA* or Δ*fhs/piaA*) (Ferreira, Neill et al., 2013) were
130 collected to investigate the extent of epithelial association and microinvasion. A positive carrier was
131 defined as colonisation at any time point (day 2 or day 6 post-inoculation), as detected by
132 microbiology culture (Weight et al., 2019). Visualisation of the mucosal cells by confocal microscopy
133 showed colonisation by the WT and mutant pneumococcal strains (Fig 1B). At day 6 post challenge,
134 compared to WT, there was no attenuation of microinvasion with either the Δ*proABC/piaA* or
135 Δ*fhs/piaA* strains, with a trend for greater microinvasion (Fig 1C) with a higher microinvasive index
136 (percentage of internalised bacteria / associated bacteria; Supplemental Information Table 1).

137

138 ***S. pneumoniae* colonisation and microinvasion of primary human airway epithelium leads to**
139 **cellular reorganisation with retention of barrier function**

140 To further explore the impact of microinvasion on epithelial biology in a complex environment, we
141 cultured *S. pneumoniae* serotype 6B WT and the isogenic biosynthesis mutants with primary normal
142 human bronchial epithelial airway (NHBE-A) cells in air-liquid interface. We observed epithelial cell
143 association and microinvasion with all three strains (Fig2A, top). TEM demonstrated that intracellular
144 bacteria for all three strains were enclosed within vacuoles (Fig 2A, bottom). As seen previously with
145 several different pneumococcal strains (Weight et al., 2019), the 6B WT and the mutant strains co-
146 localised with Junctional Adhesion Molecule A (JAM-A, Supplemental Information Fig 1A, arrow),
147 with no change in overall JAM-A expression. However, using confocal microscopy and automated
148 image analysis, for cells infected with the 6B WT strain, we did observe an increase in the intensity
149 of Zonula Occludens 1 (ZO-1) staining at the junctional membrane (Supplementary Fig 1B), and a
150 significant increase in the intensity of β catenin staining for cells infected with either the
151 Δ*proABC/piaA or* Δ*fhs/piaA* strain (Fig 2B, 2C). These changes in junctional protein expression most
152 likely occurred as a result of cellular reorganisation, as de-novo protein production would have been
153 insufficient over the 6-hour experimental infection period. As measured by transepithelial electrical
154 resistance, barrier integrity was retained over the infection period, (Fig 2D).

155

156 When cultured at an air-liquid interface, NHBE cells differentiate into a typical pseudostratified
157 columnar ciliated epithelium, consisting of goblet, Clara, basal and ciliated cells (Fig 3A). Although
158 there was no predilection by *S. pneumoniae* for particular epithelial cell-types, pneumococci were
159 observed amongst cilia (acetylated tubulin positive cells, Fig 3B and Supplemental Information Fig
160 2) and co-localised with mucus (mucin5ac positive, Fig 3C, arrows). Strikingly, while the cellular
161 composition of the epithelial cultures exposed to the Δ*fhs/piaA* strain were comparable in
162 appearance to non-infected cells by SEM, exposure to the 6B WT and Δ*proABC/piaA* strains resulted
163 in an increased abundance in secreted mucus globules compared to non-infected cells (Fig 3A).
164 This appeared to be due to differential cellular secretion of preformed mucus rather than de-novo

165 production as these differences were not reflected in an increase in the expression of the gel-forming
166 glycoprotein Mucin5AC (Fig 3C and 3E, right graph). Following infection by the Δ*proABC/piaA* strain
167 we found a significant increase in expression of acetylated tubulin (Fig 3B and 3E, left graph), which
168 has been shown to be associated with increased microtubule conformation and elasticity, and occurs
169 by post-translational modification (Eshun-Wilson, Zhang et al., 2019, Iliev, Djannatian et al., 2009).
170 In contrast, following exposure to Δ*fhs/piaA* strain, we saw an increased expression of the anti-
171 inflammatory protein, uteroglobin (UG), which is a multifunctional epithelial secreted protein with anti-
172 inflammatory and anti-chemotactic properties, and a marker for non-ciliated Clara cells (Fig 3D and
173 3F, left graph). These changes in UG expression again most likely occurred as a result of cellular
174 reorganisation, or secretion of pre-formed protein, as de-novo protein production would have been
175 insufficient to detect over the 6-hour experimental infection period.

176

177 **Δ*proABC/piaA* and Δ*fhs/piaA* mutations of *S. pneumoniae* serotype 6B do not affect**
178 **microinvasion of Detroit 562 epithelial cells**

179 Detroit 562 epithelial nasopharyngeal cells enable the analysis of these host-pathogen interactions
180 under multiple conditions, which are not feasible with the primary cell lines. We have previously
181 shown that the pattern of Detroit 562 epithelial nasopharyngeal cell microinvasion, and subsequent
182 innate immune response to *S. pneumoniae* 6B infection *in vitro* is similar to that seen in the EPHC
183 *in vivo(Weight et al., 2019)*. We therefore then used Detroit 562 cells to further characterise
184 colonisation by the WT, Δ*proABC/piaA* and/or Δ*fhs/piaA* pneumococcal strains. We found that
185 although all the strains formed colonies on the epithelial surface (Fig 4A), the isogenic mutants
186 associated less compared to 6B WT (Fig 4B). Nonetheless, microinvasion was observed with all the
187 strains (Fig 4C), with a significantly elevated micro-invasive index for the Δ*proABC/piaA* and
188 Δ*fhs/piaA* strains compared to WT (Fig 4D). Differences in microinvasion were not due to differences
189 in intracellular viability (Fig 4E) or replication (Supplemental Information Fig 3A-F). All of the single
190 and double biosynthesis genes mutants (Δ*proABC*, Δ*fhs*, Δ*proABC/piaA*, Δ*fhs/piaA*) were impaired
191 in their ability to transmigrate across the epithelium (Fig 4F). Importantly, we show that a single Δp*iaA*

192 mutation in the *S. pneumoniae* serotype 6B did not affect epithelial association, microinvasion and
193 transmigration (Fig 4B, 4C, 4F).
194

195 Consistent with our previous findings for serotype 6B(Weight et al., 2019), Detroit 562 epithelial
196 barrier function was not compromised after three hours of infection; indeed, there was a tightening
197 of the barrier evidenced by reduced FITC dextran diffusion after pneumococcal exposure (Fig 4G).
198 Pneumococcal infection had no effect on Junctional Adhesion Molecule A (JAM-A), Zonula-
199 Occludens 1 (ZO-1), Claudin 1 or Claudin 4 expression (Supplemental Fig 4). However, we did
200 observe a significant increase in epithelial β catenin expression following incubation with the
201 Δ*proABC/piaA* and Δ*fhs/piaA* strains, compared to the WT (Fig 4H, 4I).
202

203 **Δ*fhs/piaA* but not the ΔproABC/piaA mutations attenuate the pro-inflammatory epithelial**
204 **innate response to pneumococcal colonisation and microinvasion**

205 We have previously shown that the Detroit 562 cell innate immune response to *S. pneumoniae* is
206 strain dependent (Weight et al., 2019). Having found that serotype 6B biosynthesis gene mutants
207 that are attenuated for disease retain their capacity for microinvasion, we have further assessed the
208 link between colonisation, microinvasion and epithelial cell innate immunity by RNAseq. Compared
209 to non-infected cells (Fig 5A), all strains upregulated 78 core epithelial genes related to cytokine
210 signalling in immune system, NLR signalling and GPCR ligand binding. 193 genes were upregulated
211 by both the 6B WT and Δ*proABC/piaA* strains, characterised by Rhodopsin-like receptors, GPCR
212 ligand binding, cytokine signalling in Immune system, signalling by interleukins and Toll Receptor
213 cascades. Infection with the Δ*fhs/piaA* strain resulted in a markedly different transcriptomic profile
214 with modest upregulation of 254 genes, characterised by antigen processing, proteasomal
215 pathways, GTP hydrolysis, and intracellular stress responses (Fig 5A). Overall, the epithelial genes
216 that were most upregulated following infection with 6B WT or Δ*proABC/piaA* strain were similar and
217 contrasted to the reduced gene expression profile seen with the Δ*fhs/piaA* strain despite high levels
218 of cell invasion (Fig 5B). Since both mutant strains contained the *piaA* mutation, this could not

219 account for the differences seen in these responses. Together, these data demonstrate that
220 microinvasion, the innate epithelial response and disease are not necessarily linked.

221

222 Transcription factors, cellular kinases and cytokines (Fig 5C, 5D) predicted to regulate the
223 differentially expressed genes, showed the greatest difference in profile following infection with
224 Δ*fhs/piaA* strain compared to infection with 6B WT and Δ*proABC/piaA* strains. Δ*fhs/piaA* was
225 predicted to show diminished NFκB and MAPK activation and was associated with a more intrinsic
226 and epithelial repair response that included TBK1, Raf1, JAK1 kinases and IL-1 and IL-33 cytokine
227 signalling.

228

229 **Enhanced epithelial caspase 8 activity following pneumococcal infection with the wild-type**
230 **and ΔproABC/piaA strains**

231 The NLRP3 inflammasome drives programmed epithelial cell death via caspase 1, caspase 3/7 and
232 caspase 8 activity (Surabhi, Jachmann et al., 2022). Caspase activity, primarily regulated post-
233 translationally, enables a rapid response to cellular stress and pathogen-mediated activation
234 (Maekawa, Kashkar et al., 2023). In health, caspase regulation is thought to be important for mucosal
235 integrity (Gunther, Buchen et al., 2015). During bacterial pneumonia, caspase activation is thought
236 to have an important pro-inflammatory role, possibly triggered by pneumolysin (Gonzalez-Juarbe,
237 Bradley et al., 2018, Gonzalez-Juarbe, Bradley et al., 2017). We have therefore explored whether
238 the different patterns of microinvasion and epithelial reorganisation seen with the WT 6B, and mutant
239 strains are associated with differential caspase activation.

240

241 Compared to non-infected cells, infection with all strains led up to a 1.5-fold increase in epithelial
242 caspase activity 6-hour post infection (Fig 6A, dark grey bars). To test which caspases were
243 activated, we incubated infected cell cultures with either a caspase 1 inhibitor (YVAD-CHO), a
244 caspase 3/7 inhibitor (Z-VAD-FMK), or specifically measured caspase 8 activity. We found that the

245 increase was not due to caspase 1 activity (Fig 6B). Compared to non-infected cells, caspase 3/7
246 accounted for 3% and 15% of the caspase activity induced following infection with 6B WT and
247 Δ*fhs/piaA* strain respectively (Fig 6A). In contrast, Δ*proABC/piaA* strain did not induce caspase 3/7
248 activity. Significant caspase 8 activation was seen following infection with 6B WT and Δ*proABC/piaA*
249 strain, but not with the Δ*fhs/piaA* strain (Fig 6C).

250

251 Together, these data suggest differential caspase induction following infection with the different
252 strains, linking the proinflammatory profile of the 6B WT and the Δ*proABC/piaA* with caspase 8
253 activation, which we postulate may regulate pneumococcal survival and transmission during
254 colonisation in the nasopharynx.

255

256 **Deletion of the *proABC* and *fhs* genes have broad-ranging differential effects on the *S.***
257 ***pneumoniae* virulence gene expression and metabolic gene pathways when under stress**

258 We have previously found marked transcriptional differences between the WT and both mutants in
259 response to serum stress (used to represent the physiological stress found during human infection),
260 with an over three-fold increase in the number of genes upregulated by the mutant strains compared
261 to WT (Ramos-Sevillano E., 2023). Further analysis revealed that these genes include well-
262 characterised pneumococcal virulence factors such as *ply*, *nanA*, *psaA,* those regulating oxidative
263 stress such as *SpxB*, *lctO* and *adhE*, and genes involved in purine and carbohydrate metabolism
264 (Supplemental Information Table 2). Phosphotransferase systems, amino nucleotide sugar, fructose
265 and mannose and metabolic pathways were the most significantly enriched pathways in the
266 Δ*proABC* mutant under serum stress (Table 1). In contrast, competence, purine, pyruvate, metabolic
267 pathways, amino nucleotide sugar pathways and secondary metabolites were the most significantly
268 enriched pathways in the Δ*fhs* mutant under stress (Table 1). Together these data suggest that
269 deletion of the *proABC* and *fhs* genes have widespread but differential effects on *S. pneumoniae*
270 virulence and metabolism which may explain then complex phenotypes seen following epithelial
271 infection.

272

273 ***fhs* gene mutation in *S. pneumoniae* 6B is associated with increased pneumococcal hydrogen**
274 **peroxide secretion and decreased pneumolysin activity**

275

276 *S. pneumoniae* SpxB and LctO generate hydrogen peroxide (H_2O_2) which has been shown to
277 suppress ENaC-α transcription and inhibit the Na+–K+ pump, acting as an intracellular signal to
278 increase mitochondrial production of ROS (Alibayov, Scasny et al., 2022, Erttmann & Gekara, 2019).
279 We therefore postulated that differential expression of pneumococcal H_2O_2 may modulate epithelial
280 functional responses during nasopharyngeal colonisation by *S. pneumoniae* and explain the
281 differences in the epithelial innate immune response to the 6B WT, Δ*proABC/piaA* and Δ*fhs/piaA*
282 strains. To assess this, we measured H_2O_2 concentration using a luminescence-based bioassay,
283 normalising against bacterial CFU. After three and six hours, we detected significantly higher levels
284 of H_2O_2 in Δ*fhs/piaA* cultures compared to 6B WT and Δ*proABC/piaA* strains (Fig 7A). Furthermore,
285 this was not ameliorated by epithelial cell contact (Fig. 7B).

286

287 The pore forming pneumococcal toxin pneumolysin can both activate and suppress the host innate
288 immune response and mediates the haemolytic activity characteristic of the pneumococcus
289 (Periselneris, Turner et al., 2022, Terra, Plumptre et al., 2020, Zafar, Wang et al., 2017b). H_2O_2 can
290 increase the release of pneumolysin but paradoxically also negatively impairs its haemolytic activity
291 (Bazant, Ott et al., 2023). Compatible with the latter and the higher production of H_2O_2 by the Δ*fhs*
292 */piaA* strain, despite having increased expression of *ply*, red blood cell lysis was reduced for Δ*fhs*
293 strains compared to 6B WT and Δ*proABC* (Fig. 7C).

294

295 Differential pneumococcal H_2O_2 release may therefore explain at least in part, the effects of the *S.*
296 *pneumoniae* serotype 6B WT and Δ*proABC /piaA* compared to the Δ*fhs /piaA* strain on the epithelial
297 response to colonisation and microinvasion. Importantly, in the 6-hour timeframe assessed, the

298 increased H_2O_2 release the Δ*fhs /piaA* strain was not associated with epithelial cellular toxicity or
299 loss of barrier function, but was associated with increased intracellular epithelial stress response, as
300 detected by RNAseq.

301

302

303 **DISCUSSION**

304 There is considerable variation in the propensity of different *S. pneumoniae* strains to colonise the
305 human host, cause invasive disease and transmit to others (Weiser et al., 2018). During colonisation
306 of the nasopharyngeal niche, the pneumococcus was previously thought to be confined to the mucus
307 layer and the epithelial surface (Weiser et al., 2018). However, using EHPC, we have previously
308 reported that pneumococcal microinvasion occurs in healthy volunteers (Weight et al., 2019), and
309 we now show that even when using isogenic serotype 6B pneumococcal biosynthesis pathway
310 mutant strains that are attenuated for systemic disease but not for carriage, this microinvasion is
311 preserved (Ramos-Sevillano et al., 2020). We found that pneumococcal colonisation and
312 microinvasion of primary human airway epithelium led to cellular reorganisation and mucus
313 production while retaining barrier function, although the pattern of this reorganisation varied by strain.
314 Furthermore, the pro-inflammatory innate response and caspase 8 activity associated with epithelial
315 infection by *S. pneumoniae* serotype 6B were attenuated by the Δ*fhs/piaA* but not by the
316 Δ*proABC/piaA* mutation. Under stress conditions, along with presumably compensatory changes in
317 the expression of multiple metabolic pathways, the Δ*proABC* and Δ*fhs* mutations resulted in the
318 upregulation of several pneumococcal virulence factor genes (Graphical Abstract Summary).
319 Notably, the *fhs* gene mutation in *S. pneumoniae* serotype 6B was associated with increased
320 pneumococcal hydrogen peroxide secretion and decreased pneumolysin activity. Together these
321 findings suggest that despite being attenuated for disease, the metabolic changes and the increased
322 expression of pneumococcal virulence genes in response to stress may explain the preservation of
323 epithelial microinvasion by these mutants. However, although epithelial microinvasion, cellular

324 reorganisation, innate immune response, and the propensity to cause invasive disease are strain
325 dependent, these properties do not appear to be directly co-correlated.

326

327 The complexity of the interaction between *S. pneumoniae* and the mucosal epithelium was
328 highlighted through infection of our well-characterised primary epithelial cell model(Travaglini,
329 Nabhan et al., 2020). The model consisting of Clara cells (involved in secretory, xenobiotic metabolic,
330 and progenitor cell functions), goblet cells (mucus production), ciliated cells (responsible for mucus
331 and small particle transport), exhibited considerable epithelial cellular re-organisation involving β
332 catenin, acetylated tubulin and uteroglobin in response to pneumococcal infection. In a rabbit
333 pneumococcal meningitis model, increased acetylated tubulin and microtubule stabilisation was
334 attributed to pneumolysin activity(Iliev et al., 2009). Previously, using a pneumolysin deficient mutant
335 of *S. pneumoniae* serotype 4 (TIGR4), we have shown that pneumolysin is a key driver of the
336 epithelial inflammatory response to pneumococcal infection (Weight et al., 2019). We therefore
337 speculate that the differential expression of pneumolysin and H_2O_2 by the WT and mutant strains
338 may contribute to the differing patterns of epithelial reorganisation, and goblet cell mucus release
339 that we observed, and may impact on both clearance and transmission (Weiser et al., 2018).

340

341 Epithelial infection with the 6B WT and Δ*proABC/piaA* strains induced innate inflammatory pathway
342 gene expression typical of pneumococcal infection (Weight et al., 2019), including
343 cytokine/chemokines, interleukins, Toll Like Receptor and NFκB signalling, alongside apoptotic
344 transcripts such as FOXO3 and TP53. We also identified epithelial genes upregulated only during
345 WT infection, potentially related to a greater disease-causing potential. These genes are involved in
346 RNA degradation, O-linked glycosylation, wnt signalling, DNA sensing, RIG-I pathways and signal
347 transduction. In contrast, the Δ*fhs/piaA* strain activated a pro-survival and adaptation profile,
348 upregulating genes such as JUN, SMARCA4, NFAT5, KLF6 and TCF4, which are involved in
349 homeostatic signalling and chromatin remodelling (Barutcu, Lajoie et al., 2016, Herta, Bhattacharyya
350 et al., 2018), suggestive of a more tolerant response. Ultimately, these capsule-independent

351 differences in pneumococcal-epithelial interactions may shape the adaptive immune response to
352 pneumococcal colonisation (Ferreira et al., 2013, Wilson, Cohen et al., 2015), which could then
353 further influence the outcomes of both colonisation and disease. How these findings translate to
354 differences in the duration of nasopharyngeal carriage, invasiveness, transmission or clearance
355 remains to be fully determined. However, during EHPC, Δ*fhs/piaA* infection was associated with
356 increased density at day 6 post-inoculation compared the other strains (Hill H, 2023).

357

358 Importantly, while WT serotype 6B infection led to epithelial cell reorganisation (β catenin localisation
359 to the junctional membrane and mucus secretion), pneumococcal transmigration, a more pro-
360 inflammatory innate immune transcriptomic profile and increased caspase 8 activity, all indicative of
361 a robust cellular response to *S. pneumoniae*, the Δ*fhs/piaA* but not Δ*proABC/piaA* strains was
362 attenuated for many of these characteristics. This suggests that similar to the macrophage response
363 to *S. pneumoniae*, intracellular signalling by pneumococci is not the sole determinant of the epithelial
364 response to infection (Periselneris, Ercoli et al., 2019, Periselneris et al., 2022). The *proABC* operon
365 consists of three genes involved in proline biosynthesis (ProABC)(Belitsky, Brill et al., 2001). *fhs*
366 catalyses the synthesis of N10 formyl tetrahydrofolate, essential for carbon metabolism and purine
367 nucleotide biosynthesis in various bacterial species (Crowley et al., 1997, Sah, Aluri et al., 2015),
368 especially under hypoxic conditions (Aluri, Rex et al., 2015, Sah et al., 2015). It is increasingly
369 recognised that bacterial virulence and metabolism are intimately linked (Obolski, Swarthout et al.,
370 2023). Whether the distinct epithelial innate immune response to Δ*fhs/piaA* infection is due to
371 diminished epithelial NFκB and MAPK activation (potentially linked to extracellular receptor
372 engagement), reduced caspase 8 activity mediated by enhanced pneumococcal H_2O_2 release,
373 decreased pneumolysin activity, or a compensatory metabolic response to the stress remains to be
374 determined.

375

376 *S. pneumoniae* is highly adapted to colonise the human host and transmit from person to person.
377 Invasive pneumococcal disease, particularly in its most severe forms, is a dead end for the bacteria.

378 Our observation that the induction of inflammation/ innate immunity is not necessarily linked to
379 disease potential supports our proposition that microinvasion during colonisation by the
380 pneumococcus may facilitate immune evasion. As is typical of 'professional' intracellular bacterial
381 species such as *Listeria* and *Salmonella*, the resulting host response might also promote
382 transmission (Galan, 2021, Li, Wang et al., 2020). Whether the less pro-inflammatory Δ*fhs/piaA* is
383 less transmissible than the more inflammatory WT remains to be determined but this could be further
384 explored using EHPC (Connor, German et al., 2018).

385

386 In conclusion, these data further support our proposed paradigm that epithelial microinvasion by *S.*
387 *pneumoniae* in healthy people is frequent and usually does not lead to disease. Our findings highlight
388 the broad-ranging effects of even single gene mutations in pneumococcal biosynthesis pathways,
389 which may partially explain the complexity of differences between seemingly closely related strains.
390 However, strain differences in subsequent epithelial cell microinvasion, cellular reorganisation and
391 inflammatory responses are likely driven by differential expression of a range of bacterial virulence
392 and metabolic pathways that are not necessarily co-correlated with disease-causing potential. As
393 suggested by our bacterial transcriptomic data, no single pneumococcal virulence factor or group of
394 factors fully explains the differences seen between the strains under stress. The complexity of these
395 bacterial-host cell interactions is modulated by mediators such as hydrogen peroxide and
396 pneumolysin, which can have both enhancing and inhibitory effects on the epithelial cell response to
397 infection in different contexts. *S. pneumoniae* in constantly evolving, with new variants emerging
398 both due to stochastic events and under ecological pressure from numerous factors including
399 vaccines and antibiotic exposure (Lourenco, Daon et al., 2021, Watkins, Kalizang'Oma et al., 2022)
400 (Chaguza, Senghore et al., 2020). Extensive phenotyping of emerging, genotypically related
401 pneumococcal strains offers the opportunity to more effectively unravel *S. pneumoniae* pathogenesis
402 and its adaptation to the nasopharyngeal niche.

403

404 **METHODS AND PROTOCOLS**

405

406 **Bacteria**

407 The *Streptococcus pneumoniae* serotype 6B (strain BHN 418(Browall, Norman et al., 2014)) was a
408 kind gift from Prof. Birgitta Henriques Normark (Karolinska Institute). Δ*proABC/piaA* and Δ*fhs/piaA*
409 mutant strains were generated using overlap extension PCR as described by Ramos-Sevillano *et*
410 *al*(Ramos-Sevillano et al., 2020). Stocks of bacteria were stored at -80°C when bacterial growth in
411 Todd Hewitt Broth (THY) was 0.3 $O.D._{600nm}$. Aliquots were defrosted, centrifuged at 8000g for eight
412 minutes and resuspended in 1% Fetal Bovine Serum (FBS, Gibco) in MEM media (Gibco) for
413 infections. Approximately 10 bacteria were added for every epithelial cell. Colony forming units (CFU)
414 were counted by serial dilutions on horse blood agar plates (EO Labs). Starting inoculums were not
415 significantly different across strains for all assays.

416

417 **Bacterial RNA-seq sample collection, sequencing and reads**

418 Mutant pneumococcal strains (three biological replicates for each mutant) and 6B WT (three
419 biological replicates) were grown in THY to mid log phase and the pellets resuspended in THY and
420 undiluted human serum for 60mins. The culture was then pelleted, and RNA stored in RNA Protect
421 at -70°C before extracting total RNA (Ramos-Sevillano E., 2023). Total RNA from each library was
422 ribo-depleted and sent for Illumina Next Seq Sequencing Pathogen Genomics Unit (PGU), UCL. The
423 quality of raw FASTQ reads was checked by FastQC v0.11.5, Babraham Bioinformatics, UK (S.,
424 2010) and visualised using multiQC v1.9 (Ewels, Magnusson et al., 2016). Reads were trimmed
425 using Trimmomatic 0.39 (Bolger, Lohse et al., 2014). Trimmed reads were also checked by FastQC
426 and multiQC. Trimmed reads were then mapped to KEGG annotated 6B genome sequence (670-
427 6B, Accession: CP002176.1) using bowtie2 with default settings(Langmead & Salzberg, 2012).
428 Conversion into BAM files was performed using SAMtools (Li, Handsaker et al., 2009). Mapped
429 reads were visualized in the Integrated Genome Browser (IGB) (Nicol, Helt et al., 2009).
430 FeatureCounts v2.0.0 was used to summarize read counts for each annotated feature in the
431 respective reference genomes in multimapping mode (-M) (Liao, Smyth et al., 2014).

432

433 **Differential gene expression analyses**

434 The generated count matrix was imported into R-studio (R v3.4.2) and normalization of counts and
435 differential gene expression analysis was performed by DESeq2 (Love, Huber et al., 2014). DESeq2
436 normalized libraries were regularized log transformed for visualizing heatmaps and clustering.
437 Differential gene expression was performed on raw counts. Fold change shrinkage was implemented
438 with the apeglm package within DESeq2. Genes with a log2 fold change > 1.5 and false discovery
439 rate (FDR) of < 0.05 were categorized as differentially expressed. KEGG pathway enrichment and
440 module analysis were performed on differentially regulated genes using over representation analysis
441 (ORA) implemented by clusterProfiler (Yu, Wang et al., 2012).

442

443 **Experimental Human Pneumococcal Carriage Model (EHPC)**

444 A full explanation of experimental design and selection criteria has been previously described
445 (Weight et al., 2019). Following written informed consent, healthy non-smoking adults between the
446 ages of 18 – 59 were inoculated with 80,000 CFU/nostril live strains of *S. pneumoniae*. Mucosal cells
447 from the inferior turbinate using a plastic Rhino-probe™ (curettage, Arlington Scientific) were
448 collected prior to inoculation, and days 2 and 6 post-inoculation. Samples were processed for
449 confocal microscopy analysis. Nasal wash samples were collected for CFU count analysis. There
450 were no adverse events. Ethical approval was given by NHS Research and Ethics Committee
451 (REC)/Liverpool School of Tropical Medicine (LSTM) REC, reference number: 18/NW/0481 and
452 Human Tissue Authority licensing number 12548.

453

454 **Primary Human Epithelial Cells**

455 Normal Human Primary Bronchial/Tracheal Epithelial Cells (NHBE-A, ATCC® PCS-300-010™) were
456 plated at $6x10^3$ cells/cm^2 on a layer of sub-lethally γ-irradiated (60 Gy) mouse embryonic fibroblasts
457 3T3-J2 cells (kind donation from Howard Green, Harvard Medical School, Boston(Rheinwald &
458 Green, 1975)) with keratinocyte culture medium cFAD (3:1 DMEM (Gibco) to Ham F-12 Nut Mix

459 (Gibco), 10% FBS (HyClone, Sigma), 1% Penicillin-Streptomycin (100X, Sigma), 0.4 µg/mL
460 Hydrocortisone (Calbiochem, USA), 5 µg/ml Insulin (various), 10-10 Cholera Toxin (Sigma) and
461 2x10-9 Triodothyronine (Sigma)). Epithelial cells were stimulated with 10 ng/mL human epidermal
462 growth factor (hEGF, PeproTech, USA) on days 3 and 5. Cultures were grown at 37°C 6% CO_2 and
463 sub-confluent cultures were trypsinised with 0.25% Trypsin-EDTA (Sigma). For NHBE-A
464 differentiation in Air Liquid Interface (ALI) culture, cells were plated at a density of $6x10^4/cm^2$ on 1µm
465 pore PET cell culture inserts (12 wells, Greiner). The insert was supplemented with cFAD medium
466 on the top and bottom. After 48 hours, medium was removed from the top of the culture (exposure)
467 and the culture was fed with fresh PneumaCult™ differentiation Medium (Stemcell Technologies)
468 from the bottom of the well every 2 days for 3 weeks, until cell ciliation was observed. Antibiotics
469 were removed from the medium and cells washed 24 hours before infection experiments.

470

471 **Human Epithelial Cell Lines**

472 Human pharyngeal carcinoma Detroit 562 epithelial cells (ATCC_CCL-138) were grown in 10% FCS
473 in alpha MEM media (Gibco). For each set of experiments, cells were used within 5 passages. Cells
474 consistently tested PCR negative for mycoplasma (Cambridge Biosciences).

475

476 **Pneumococcal-epithelial cell co-culture**

477 For association and internalisation assays, confluent monolayers of Detroit 562 cells (typically day 7
478 - 8 post plating) cultured on 12 well plates (Corning), were exposed to *S. pneumoniae* (1 cell : 10
479 pneumococci) for three hours in 1% FCS alpha MEM (six-hour infection for HNBE-A cells in 1%
480 Pneumocult media without supplements) (Weight et al., 2019). Cells washed three times in $HBSS^{+/+}$
481 before incubation in 1% saponin for 10 minutes at 37°C to lyse cells. Bacterial dilutions were plated
482 on horse blood agar for 16 hours and colony forming units counted. For internalisation quantification,
483 200µg/ml gentamicin was added to the cells for one hour before incubation with saponin.

484

485 For transmigration assays, Detroit 562 cells were plated onto 3µm pore, PET Transwell Inserts
486 (ThermoFisher) typically for 10 days (Weight et al., 2019). Media was changed to 1% FCS (250µl

487 apical chamber, 1ml basal chamber) one hour prior to infection experiments. 1mg/ml FITC-dextran
488 (Sigma Aldrich) was added to the apical chamber of selected inserts for permeability assays.
489 Transepithelial Electrical Resistance (TEER) was measured before and after infection using an
490 EVOM2 (World Precision Instruments). Bacteria were added to the cells for three hours during of
491 which 50µl of basal media was repeatedly removed to measure bacterial load by counting CFU/well.
492 Permeability was recorded using a FLUOstar Omega (BMG Labtech) at 488nm.
493
494 **Confocal Microscopy**
495 Sample processing was performed as previously described(Weight et al., 2019). Briefly, mucosal
496 cells from the EHPC model were placed directly into 4% PFA and cytospun onto microscope slides.
497 NHBE-A cells and Detroit 562 cells cultured on transwell membranes were fixed in 4% PFA (Pierce,
498 Methanol Free). Cells were permeabilised with 0.2% Triton X-100 for 10 minutes, blocked for one
499 hour in blocking buffer (3% goat serum and 3% BSA in PBS (Sigma)) and incubated with
500 pneumococcal antisera Pool Q (raised against the polysaccharide capsule, SSI Diagnostica) for one
501 hour. Wheat germ agglutinin conjugated to Rhodamine (Vector Labs) was added along with goat-
502 anti rabbit IgG conjugated to Alexa Fluor 488 for 45 minutes in blocking buffer. Primary (used at
503 1:100) antibodies used for epithelial cell proteins can be found in Supplemental Information Table 3.
504 Secondary (used at 1:500) antibodies were either goat anti-mouse or goat anti-rabbit – Alexa Fluor
505 555 or 546, ThermoFisher. Of note, for epithelial protein antibodies raised in rabbit (Uteroglobin), no
506 pneumococcal staining was possible and therefore pneumococci were not visible on the images.
507 DAPI was added for 5 minutes and cells were mounted with Aqua PolyMount (VWR International)
508 and a coverslip on the microslide. Pneumococci were recorded by manual scanning of the whole
509 cytospin for the EHPC samples. More than three fields of view were recorded for each bacterial
510 strain for Detroit 562 cell infections, using inverted Zeiss LSM (either 700 or 880) confocal
511 microscopes. Images were processed with Zeiss LSM Image Browser. Z stacks were recorded at
512 1µm intervals at either 40x oil or 63x oil objectives. Automated image analysis was carried out using
513 Cellprofiler (Carpenter, Jones et al., 2006).
514

515 **Electron Microscopy**

516 Preparation of Detroit 562 cells and NHBE-A cells was identical, and previously described(Weight et
517 al., 2019). Briefly, cells cultured on transwells were fixed with 2% paraformaldehyde and 1.5%
518 glutaraldehyde in 0.1 M cacodylate buffer and post-fixed in 1% OsO4 / 1.5% K4Fe(CN)6 in 0.1 M
519 cacodylate buffer pH7.3. Samples were dehydrated in graded ethanol-water series and infiltrated
520 with Agar 100 resin mix. Ultra-thin sections were cut at 70-80 nm using a diamond knife on a Reichert
521 ultracut microtome. Sections were collected on 300 mesh copper grids and stained with lead citrate.
522 For transmission electron microscopy the samples were hardened at 60°C for 48 hours. The
523 coverslip was removed, and a representative area was selected. Ultra-thin sections were cut at 70-
524 80 nm using a diamond knife on a Reichert ultra-cut S microtome. Sections were collected on copper
525 grids and stained with lead citrate. Samples were viewed with a Joel 1010 transition electron
526 microscope and the images recorded using a Gatan Orius CCD camera.

527

528 **Pneumolysin activity**

529 Adapted from Kirkham et al(Kirkham, Kerr et al., 2006). Briefly, final concentration of 2% horse blood
530 (EO Labs) solution was prepared in phenol free alpha MEM (Life Technologies) and 100 µl added
531 to wells of a 96 U-bottom plate (Corning). 100 µl of bacterial solutions (containing ~$2.5x10^6$ bacteria)
532 were suspended in phenol free alpha MEM were added to each 96 well. Saponin was used as a
533 positive control for lysis. Solutions were incubated for 30 minutes at 37°C before centrifugation at
534 1000g for one minute. 100 µl was transferred into a new 96 well plate and absorbance recorded at
535 540nm on a plate reader.

536

537 **Hydrogen Peroxide Assay**

538 Detroit 562 cells were cultured in white 96 well plates (Corning). NHBE-A cells were cultured in 12
539 well plates in Pneumocult media. Cells were incubated with H_2O_2 substrate and infected with strains
540 of *S. pneumoniae* for up to six hours according to manufacturers' instructions (ROS-Glo™ H_2O_2
541 Assay, Promega). ROS-Glo™ Detection solution was added to the cells and incubated for 20
542 minutes. For primary cells, supernatant was then transferred to a white 96 well plate. Luminescence
543 was read using a GloMax -Multi Detection System plate reader (Promega).

544

545 **Caspase assay**

546 Detroit 562 cells were cultured in white 96 well plates (Corning). NHBE-A cells were cultured in 12
547 well plates in Pneumocult media. Cells were infected with strains of *S. pneumoniae* for up to six
548 hours. Primary cell supernatant was transferred to a white 96 well plate. Samples were incubated
549 with Caspase-Glo® 1 Reagent, Caspase-Glo® 1 YVAD-CHO Reagent, Caspase-Glo® Z-VAD-FMK
550 Reagent or Caspase-Glo® 8 Reagent, for one hour and according to manufacturers' instructions
551 (Promega). Luminescence was read using a GloMax-Multi Detection System plate reader
552 (Promega).

553

554 RNA samples and sequencing (RNA-Seq)

555 RNA-Seq data was collected as previously described (3). Confluent monolayers of Detroit 562
556 epithelial cells were infected with S. pneumoniae strains for four hours before collection in RNALater.
557 RNA was extracted using a Qiagen RNAEasy micro kit and treated for DNA removal using a Qiagen
558 Turbo DNA-free kit. RNA quality was assessed and quantified using a BioAnalyser (Agilent 2100).
559 Samples were sequenced using Illumina Nextseq 500/550 High Output 75 cycle kit giving 15-20
560 million 41bp paired-end reads per sample (Pathogens Genomic Unit, UCL).

561

562 **Statistics**

563 Each condition within each experiment was performed in duplicate or triplicate, and each experiment
564 was performed independently more than three times, unless stated otherwise. Error bars represent
565 SEM, unless stated otherwise. GraphPad Prism Version 7 was used for parametric (t-tests or
566 ANOVA) or non-parametric (Mann-Whitney or Kruskal-Wallis tests) analysis, which was based on
567 the Shapiro-Wilk normality test. Ad hoc tests were performed using Tukey's (for parametric data) or
568 Dunn's (for non-parametric data) multiple comparisons test. P values less than 0.05 were considered
569 significant.

570

571 **Data and code availability**

572 Source data are provided as a Source Data file. RNAseq data from the Detroit 562 cell infections is
573 publicly accessible through Zenodo with Accession (DOI:10.5281/zenodo.7997789).

574

575 **ACKNOWLEDGEMENTS**

576 This study was funded by CMW from a Postdoctoral Innovation Award from UCL, a Pump-Priming
577 Award and Enhancement Award from the Human Infection Challenge Network for Vaccine
578 Development (HIC-VAC (funded by the GCRF Networks in Vaccines Research and Development)
579 which is co-funded by the MRC and BBSRC). This UK funded award is part of the EDCTP2
580 programme supported by the European Union. CMW and RSH are supported by the Medical
581 Research Council (grant MR/T016329/1). The authors would like to thank Prof. Peter Hermans
582 (Radboud University Medical Centre) for donating the 6B pneumococcal strain originally from Prof.
583 Birgitta Henriques-Normark (Karolinska Institute) and obtained directly from DF at LSTM. EHPC
584 sample collection was supported by the Medical Research Council (grant MR/M011569/1), Bill and
585 Melinda Gates Foundation (grant OPP1117728) awarded to DF and the National Institute for Health
586 Research (NIHR) Local Comprehensive Research Network. The authors also wish to thank the
587 EHPC Clinical Team at LSTM and all the volunteers. Confocal imaging facilities at LSTM were
588 funded by a Wellcome Trust Multi-User Equipment Grant (104936/Z/14/Z). Electron microscopy
589 processing and image capture was performed by Dr. Elizabeth Slavik-Smith in the Biosciences EM
590 facility at UCL. MC is supported by a Springboard to Independence grant (AirwayStasis) from the
591 French Government's Investissement d'Avenir program, the Laboratoire d'Excellence ''Integrative
592 Biology of Emerging Infectious Diseases" (ANR-10-LABX-62-IBEID) and the Chromatin and infection
593 unit headed by Melanie A. Hamon. RNA-Seq library preparation was undertaken at UCL through the
594 UCL/UCLH Biomedical Research Centre and MRC funded Pathogen Genomics Unit (PGU,
595 G0900950). All RNAseq data processing was completed by the PGU. MN is supported by the
596 Wellcome Trust and by NIHR Biomedical Research Centre Funding to University College Hospitals
597 NHS Foundation Trust and University College London. RR is supported by Marie Skłodowska-Curie
598 Individual Fellowships 896014. PB is supported by the European Research Council (ERC-Stg No.

639429), the Rosetrees Trust (M362-F1; M553), the CF Trust (SRC006;SRC020), the London Advanced Therapies - Research England (C2N-AT.006), the MRC Confidence in Concept scheme (Award: MC_PC_17180), the Innovate UK (Smart grant n.10005465), the Duchenne Parent Project (DPP) and the NIHR GOSH BRC. MW is supported by a 223065 Wellcome Investigator Award to Clare Jolly, UCL. ERS and JSB are supported by MRC grant R/N02687X/1 and Wellcome grant 221803/Z/20/Z. JSB is partially supported by the Department of Health's National Institute of Health and Care Research Biomedical Research Centre funding to UCLH. RSH is a NIHR Senior Investigator.

AUTHOR CONTRIBUTIONS: CMW conceived, funded, designed and conducted the study, performed the experiments, acquired samples and processed data, and wrote the first draft of the manuscript. GP analysed and interpreted the RNAseq data. MB analysed and interpreted the bacterial transcriptomic data. RR cultured and differentiated primary epithelial cells. ERS generated the 6B mutant strains and bacterial transcriptomic data. JR collected and processed EHPC samples. JAGA processed the RNA-Seq data. MW ran the image analysis. MC provided technical advice. PB and CJ provided investigator support. MN provided RNA-Seq analysis support. DF provided investigator support and EHPC clinical samples. JSB generated the 6B mutant strains, interpreted the data and revised the manuscript. RSH provided investigator support, designed and interpreted the data, revised the manuscript. All authors commented on and approved the manuscript.

COMPETING INTERESTS: The authors declare no competing interests.

REFERENCES

Alibayov B, Scasny A, Khan F, Creel A, Smith P, Vidal AGJ, Fitisemanu FM, Padilla-Benavides T, Weiser JN, Vidal JE (2022) Oxidative Reactions Catalyzed by Hydrogen Peroxide Produced by Streptococcus pneumoniae and Other Streptococci Cause the Release and Degradation of Heme from Hemoglobin. Infect Immun 90: e0047122

Aluri S, Rex K, Varshney U (2015) Simultaneous presence of fhs and purT genes is disadvantageous for the fitness of Escherichia coli growth. FEMS Microbiol Lett 362

628 Amin-Chowdhury Z, Collins S, Sheppard C, Litt D, Fry NK, Andrews N, Ladhani SN (2020) Characteristics of
629 Invasive Pneumococcal Disease Caused by Emerging Serotypes After the Introduction of the 13-Valent
630 Pneumococcal Conjugate Vaccine in England: A Prospective Observational Cohort Study, 2014-2018. Clin
631 Infect Dis 71: e235-e243
632 Barutcu AR, Lajoie BR, Fritz AJ, McCord RP, Nickerson JA, van Wijnen AJ, Lian JB, Stein JL, Dekker J, Stein GS,
633 Imbalzano AN (2016) SMARCA4 regulates gene expression and higher-order chromatin structure in
634 proliferating mammary epithelial cells. Genome Res 26: 1188-201
635 Bazant J, Ott B, Hudel M, Hain T, Lucas R, Mraheil MA (2023) Impact of Endogenous Pneumococcal Hydrogen
636 Peroxide on the Activity and Release of Pneumolysin. Toxins (Basel) 15
637 Belitsky BR, Brill J, Bremer E, Sonenshein AL (2001) Multiple genes for the last step of proline biosynthesis in
638 Bacillus subtilis. J Bacteriol 183: 4389-92
639 Bolger AM, Lohse M, Usadel B (2014) Trimmomatic: a flexible trimmer for Illumina sequence data.
640 Bioinformatics 30: 2114-20
641 Brill J, Hoffmann T, Bleisteiner M, Bremer E (2011) Osmotically controlled synthesis of the compatible solute
642 proline is critical for cellular defense of Bacillus subtilis against high osmolarity. J Bacteriol 193: 5335-46
643 Browall S, Norman M, Tangrot J, Galanis I, Sjostrom K, Dagerhamn J, Hellberg C, Pathak A, Spadafina T,
644 Sandgren A, Battig P, Franzen O, Andersson B, Ortqvist A, Normark S, Henriques-Normark B (2014) Intraclonal
645 variations among Streptococcus pneumoniae isolates influence the likelihood of invasive disease in children.
646 J Infect Dis 209: 377-88
647 Brown JS, Gilliland SM, Holden DW (2001) A Streptococcus pneumoniae pathogenicity island encoding an
648 ABC transporter involved in iron uptake and virulence. Mol Microbiol 40: 572-85
649 Carpenter AE, Jones TR, Lamprecht MR, Clarke C, Kang IH, Friman O, Guertin DA, Chang JH, Lindquist RA,
650 Moffat J, Golland P, Sabatini DM (2006) CellProfiler: image analysis software for identifying and quantifying
651 cell phenotypes. Genome Biol 7: R100
652 Chaguza C, Senghore M, Bojang E, Gladstone RA, Lo SW, Tientcheu PE, Bancroft RE, Worwui A, Foster-Nyarko
653 E, Ceesay F, Okoi C, McGee L, Klugman KP, Breiman RF, Barer MR, Adegbola RA, Antonio M, Bentley SD,
654 Kwambana-Adams BA (2020) Within-host microevolution of Streptococcus pneumoniae is rapid and adaptive
655 during natural colonisation. Nat Commun 11: 3442
656 Connor V, German E, Pojar S, Mitsi E, Hales C, Nikolaou E, Hyder-Wright A, Adler H, Zaidi S, Hill H, Jochems
657 SP, Burhan H, French N, Tobery T, Rylance J, Ferreira DM (2018) Hands are vehicles for transmission of
658 Streptococcus pneumoniae in novel controlled human infection study. Eur Respir J 52
659 Crowley PJ, Gutierrez JA, Hillman JD, Bleiweis AS (1997) Genetic and physiologic analysis of a formyl-
660 tetrahydrofolate synthetase mutant of Streptococcus mutans. J Bacteriol 179: 1563-72
661 Echlin H, Frank M, Rock C, Rosch JW (2020) Role of the pyruvate metabolic network on carbohydrate
662 metabolism and virulence in Streptococcus pneumoniae. Mol Microbiol 114: 536-552
663 Erttmann SF, Gekara NO (2019) Hydrogen peroxide release by bacteria suppresses inflammasome-dependent
664 innate immunity. Nat Commun 10: 3493
665 Eshun-Wilson L, Zhang R, Portran D, Nachury MV, Toso DB, Lohr T, Vendruscolo M, Bonomi M, Fraser JS,
666 Nogales E (2019) Effects of alpha-tubulin acetylation on microtubule structure and stability. Proc Natl Acad
667 Sci U S A 116: 10366-10371
668 Ewels P, Magnusson M, Lundin S, Kaller M (2016) MultiQC: summarize analysis results for multiple tools and
669 samples in a single report. Bioinformatics 32: 3047-8
670 Ferreira DM, Neill DR, Bangert M, Gritzfeld JF, Green N, Wright AK, Pennington SH, Bricio-Moreno L, Moreno
671 AT, Miyaji EN, Wright AD, Collins AM, Goldblatt D, Kadioglu A, Gordon SB (2013) Controlled human infection
672 and rechallenge with Streptococcus pneumoniae reveals the protective efficacy of carriage in healthy adults.
673 Am J Respir Crit Care Med 187: 855-64
674 Galan JE (2021) Salmonella Typhimurium and inflammation: a pathogen-centric affair. Nat Rev Microbiol 19:
675 716-725
676 Gladstone RA, Lo SW, Lees JA, Croucher NJ, van Tonder AJ, Corander J, Page AJ, Marttinen P, Bentley LJ,
677 Ochoa TJ, Ho PL, du Plessis M, Cornick JE, Kwambana-Adams B, Benisty R, Nzenze SA, Madhi SA, Hawkins PA,
678 Everett DB, Antonio M et al. (2019) International genomic definition of pneumococcal lineages, to
679 contextualise disease, antibiotic resistance and vaccine impact. EBioMedicine 43: 338-346

680 Gonzalez-Juarbe N, Bradley KM, Riegler AN, Reyes LF, Brissac T, Park SS, Restrepo MI, Orihuela CJ (2018)
681 Bacterial Pore-Forming Toxins Promote the Activation of Caspases in Parallel to Necroptosis to Enhance
682 Alarmin Release and Inflammation During Pneumonia. Sci Rep 8: 5846
683 Gonzalez-Juarbe N, Bradley KM, Shenoy AT, Gilley RP, Reyes LF, Hinojosa CA, Restrepo MI, Dube PH, Bergman
684 MA, Orihuela CJ (2017) Pore-forming toxin-mediated ion dysregulation leads to death receptor-independent
685 necroptosis of lung epithelial cells during bacterial pneumonia. Cell Death Differ 24: 917-928
686 Gunther C, Buchen B, He GW, Hornef M, Torow N, Neumann H, Wittkopf N, Martini E, Basic M, Bleich A,
687 Watson AJ, Neurath MF, Becker C (2015) Caspase-8 controls the gut response to microbial challenges by Tnf-
688 alpha-dependent and independent pathways. Gut 64: 601-10
689 Hartel T, Eylert E, Schulz C, Petruschka L, Gierok P, Grubmuller S, Lalk M, Eisenreich W, Hammerschmidt S
690 (2012) Characterization of central carbon metabolism of Streptococcus pneumoniae by isotopologue
691 profiling. J Biol Chem 287: 4260-74
692 Henriques-Normark B, Tuomanen EI (2013) The pneumococcus: epidemiology, microbiology, and
693 pathogenesis. Cold Spring Harb Perspect Med 3
694 Herta T, Bhattacharyya A, Bollensdorf C, Kabus C, Garcia P, Suttorp N, Hippenstiel S, Zahlten J (2018) DNA-
695 release by Streptococcus pneumoniae autolysin LytA induced Krueppel-like factor 4 expression in
696 macrophages. Sci Rep 8: 5723
697 Hill H ME, Nikolaou E, Blizard A, Pojar S, Howard A, Hyder-Wright A, Devin J, Reiné J, Robinson R, Solórzano
698 C, Jochems S, Kenny-Nyazika T, Ramos-Sevillano E, Weight CM, Myerscough C, McLennan D, MortonB ,
699 Gibbons E, Farrar M, Randles V, Burhan H, Chen T, Shandling AD, Campo JJ, Heyderman RS, Gordon SB, Brown
700 JS, Collins AM, Ferreira DM (2023) A Randomised Controlled Trial of Nasal Immunisation with Live Virulence
701 Attenuated Streptococcus pneumoniae Strains using Human Infection Challenge. Medrxiv
702 Hill H, Mitsi E, Nikolaou E, Blizard A, Pojar S, Howard A, Hyder-Wright A, Devin J, Reine J, Robinson R,
703 Solorzano C, Jochems SP, Kenny-Nyazika T, Ramos-Sevillano E, Weight CM, Myerscough C, McLenaghan D,
704 Morton B, Gibbons E, Farrar M et al. (2023) A Randomised Controlled Trial of Nasal Immunisation with Live
705 Virulence Attenuated Streptococcus pneumoniae Strains Using Human Infection Challenge. Am J Respir Crit
706 Care Med
707 Iliev AI, Djannatian JR, Opazo F, Gerber J, Nau R, Mitchell TJ, Wouters FS (2009) Rapid microtubule bundling
708 and stabilization by the Streptococcus pneumoniae neurotoxin pneumolysin in a cholesterol-dependent,
709 non-lytic and Src-kinase dependent manner inhibits intracellular trafficking. Mol Microbiol 71: 461-77
710 Kirkham LA, Kerr AR, Douce GR, Paterson GK, Dilts DA, Liu DF, Mitchell TJ (2006) Construction and
711 immunological characterization of a novel nontoxic protective pneumolysin mutant for use in future
712 pneumococcal vaccines. Infect Immun 74: 586-93
713 Kohler S, Voss F, Gomez Mejia A, Brown JS, Hammerschmidt S (2016) Pneumococcal lipoproteins involved in
714 bacterial fitness, virulence, and immune evasion. FEBS Lett 590: 3820-3839
715 Langmead B, Salzberg SL (2012) Fast gapped-read alignment with Bowtie 2. Nat Methods 9: 357-9
716 Li G, Wang G, Li M, Li L, Liu H, Sun M, Wen Z (2020) Morin inhibits Listeria monocytogenes virulence in vivo
717 and in vitro by targeting listeriolysin O and inflammation. BMC Microbiol 20: 112
718 Li H, Handsaker B, Wysoker A, Fennell T, Ruan J, Homer N, Marth G, Abecasis G, Durbin R, Genome Project
719 Data Processing S (2009) The Sequence Alignment/Map format and SAMtools. Bioinformatics 25: 2078-9
720 Liao Y, Smyth GK, Shi W (2014) featureCounts: an efficient general purpose program for assigning sequence
721 reads to genomic features. Bioinformatics 30: 923-30
722 Lourenco J, Daon Y, Gori A, Obolski U (2021) Pneumococcal Competition Modulates Antibiotic Resistance in
723 the Pre-Vaccination Era: A Modelling Study. Vaccines (Basel) 9
724 Love MI, Huber W, Anders S (2014) Moderated estimation of fold change and dispersion for RNA-seq data
725 with DESeq2. Genome Biol 15: 550
726 Maekawa T, Kashkar H, Coll NS (2023) Dying in self-defence: a comparative overview of immunogenic cell
727 death signalling in animals and plants. Cell Death Differ 30: 258-268
728 Mahdi LK, Wang H, Van der Hoek MB, Paton JC, Ogunniyi AD (2012) Identification of a novel pneumococcal
729 vaccine antigen preferentially expressed during meningitis in mice. J Clin Invest 122: 2208-20
730 Nicol JW, Helt GA, Blanchard SG, Jr., Raja A, Loraine AE (2009) The Integrated Genome Browser: free software
731 for distribution and exploration of genome-scale datasets. Bioinformatics 25: 2730-1

732 O'Brien KL, Wolfson LJ, Watt JP, Henkle E, Deloria-Knoll M, McCall N, Lee E, Mulholland K, Levine OS, Cherian
733 T, Hib, Pneumococcal Global Burden of Disease Study T (2009) Burden of disease caused by Streptococcus
734 pneumoniae in children younger than 5 years: global estimates. Lancet 374: 893-902
735 Obolski U, Swarthout TD, Kalizang'oma A, Mwalukomo TS, Chan JM, Weight CM, Brown C, Cave R, Cornick J,
736 Kamng'ona AW, Msefula J, Ercoli G, Brown JS, Lourenco J, Maiden MC, French N, Gupta S, Heyderman RS
737 (2023) The metabolic, virulence and antimicrobial resistance profiles of colonising Streptococcus
738 pneumoniae shift after PCV13 introduction in urban Malawi. Nat Commun 14: 7477
739 Ogunniyi AD, Mahdi LK, Trappetti C, Verhoeven N, Mermans D, Van der Hoek MB, Plumptre CD, Paton JC
740 (2012) Identification of genes that contribute to the pathogenesis of invasive pneumococcal disease by in
741 vivo transcriptomic analysis. Infect Immun 80: 3268-78
742 Periselneris J, Ercoli G, Pollard T, Chimalapati S, Camberlein E, Szylar G, Hyams C, Tomlinson G, Petersen FC,
743 Floto RA, Noursadeghi M, Brown JS (2019) Relative Contributions of Extracellular and Internalized Bacteria
744 to Early Macrophage Proinflammatory Responses to Streptococcus pneumoniae. mBio 10
745 Periselneris J, Turner CT, Ercoli G, Szylar G, Weight CM, Thurston T, Whelan M, Tomlinson G, Noursadeghi M,
746 Brown J (2022) Pneumolysin suppresses the initial macrophage pro-inflammatory response to Streptococcus
747 pneumoniae. Immunology 167: 413-427
748 Ramos-Sevillano E, Ercoli G, Felgner P, Ramiro de Assis R, Nakajima R, Goldblatt D, Heyderman RS, Gordon
749 SB, Ferreira DM, Brown JS (2020) Preclinical Development of Virulence Attenuated Streptococcus
750 pneumoniae Strains Able to Enhance Protective Immunity Against Pneumococcal Infection. Am J Respir Crit
751 Care Med
752 Ramos-Sevillano E. EG, Guerra-Assunção J.F., Betts M., Partridge F., Fernandes V.E., Wall E., Gordon S.B.,
753 Ferreira D.M., Heyderman R.S., Brown J.S. (2023) Essential role of proline synthesis and the one-carbon
754 metabolism pathways for systemic virulence of Streptococcus pneumoniae. Biorxiv
755 Rheinwald JG, Green H (1975) Serial cultivation of strains of human epidermal keratinocytes: the formation
756 of keratinizing colonies from single cells. Cell 6: 331-43
757 S. A (2010) FastQC: a quality control tool for high throughput sequence data.
758 Sah S, Aluri S, Rex K, Varshney U (2015) One-carbon metabolic pathway rewiring in Escherichia coli reveals
759 an evolutionary advantage of 10-formyltetrahydrofolate synthetase (Fhs) in survival under hypoxia. J
760 Bacteriol 197: 717-26
761 Surabhi S, Jachmann LH, Shumba P, Burchhardt G, Hammerschmidt S, Siemens N (2022) Hydrogen Peroxide
762 Is Crucial for NLRP3 Inflammasome-Mediated IL-1beta Production and Cell Death in Pneumococcal Infections
763 of Bronchial Epithelial Cells. J Innate Immun 14: 192-206
764 Terra VS, Plumptre CD, Wall EC, Brown JS, Wren BW (2020) Construction of a pneumolysin deficient mutant
765 in streptococcus pneumoniae serotype 1 strain 519/43 and phenotypic characterisation. Microb Pathog 141:
766 103999
767 Travaglini KJ, Nabhan AN, Penland L, Sinha R, Gillich A, Sit RV, Chang S, Conley SD, Mori Y, Seita J, Berry GJ,
768 Shrager JB, Metzger RJ, Kuo CS, Neff N, Weissman IL, Quake SR, Krasnow MA (2020) A molecular cell atlas of
769 the human lung from single-cell RNA sequencing. Nature 587: 619-625
770 van Opijnen T, Camilli A (2012) A fine scale phenotype-genotype virulence map of a bacterial pathogen.
771 Genome Res 22: 2541-51
772 Watkins ER, Kalizang'Oma A, Gori A, Gupta S, Heyderman RS (2022) Factors affecting antimicrobial resistance
773 in Streptococcus pneumoniae following vaccination introduction. Trends Microbiol 30: 1135-1145
774 Weight CM, Venturini C, Pojar S, Jochems SP, Reine J, Nikolaou E, Solorzano C, Noursadeghi M, Brown JS,
775 Ferreira DM, Heyderman RS (2019) Microinvasion by Streptococcus pneumoniae induces epithelial innate
776 immunity during colonisation at the human mucosal surface. Nat Commun 10: 3060
777 Weiser JN, Ferreira DM, Paton JC (2018) Streptococcus pneumoniae: transmission, colonization and invasion.
778 Nat Rev Microbiol 16: 355-367
779 Wilson R, Cohen JM, Jose RJ, de Vogel C, Baxendale H, Brown JS (2015) Protection against Streptococcus
780 pneumoniae lung infection after nasopharyngeal colonization requires both humoral and cellular immune
781 responses. Mucosal Immunol 8: 627-39
782 Yu G, Wang LG, Han Y, He QY (2012) clusterProfiler: an R package for comparing biological themes among
783 gene clusters. OMICS 16: 284-7

784 Zafar MA, Hamaguchi S, Zangari T, Cammer M, Weiser JN (2017a) Capsule Type and Amount Affect Shedding
785 and Transmission of Streptococcus pneumoniae. mBio 8
786 Zafar MA, Wang Y, Hamaguchi S, Weiser JN (2017b) Host-to-Host Transmission of Streptococcus pneumoniae
787 Is Driven by Its Inflammatory Toxin, Pneumolysin. Cell Host Microbe 21: 73-83

788

789

790 **FIGURE LEGENDS**

791 **Table 1. Differentially expressed pathways from single isogenic mutants in human**
792 **serum compared to WT.** 55 genes were selected within competence pathways, amino acid
793 metabolism, virulence factors, oxidative stress pathways and other known genes important
794 for colonisation, for assessment of changes in gene expression following serum stress. *q-*
795 *value* measures the proportion of false positives incurred (the false discovery rate) when
796 that particular test is significant.

797

798 **Fig 1. Pneumococcal – epithelial interactions in the EHPC model**. (A) Schematic showing that
799 during colonisation, pneumococci adhere to the epithelial cell surface (association), internalise inside
800 epithelial cells (microinvasion). Mucus – lime; pneumococci – purple; intracellular vacuole – dark
801 green; epithelial cells – yellow; nucleus – brown; cell junctions – pink. (B) Representative microscopy
802 images showing 6B association to the epithelium and microinvasion by the Δ*proABC/piaA* or
803 Δ*fhs/piaA* mutants. Surface carbohydrates (red), nuclei (DAPI, blue), pneumococci (green). (C)
804 Table summarising the percentage of bacteria that were found by microscopy, on the surface
805 (association) or inside (microinvasion) cells in the EHPC model. Mucosal curettage samples were
806 collected at day 6 post-pneumococcal challenge. Number of volunteers (n) in each group is indicated
807 in brackets, along with the total numbers of pneumococci (Spn) counted.

808

809 **Fig 2. Impact of pneumococcal infection on NHBE-A cell junctional protein expression and**
810 **barrier integrity.** NHBE-A Cells were cultured at ALI and infected with pneumococcal strains for

811 6hrs. (A) Top: Representative confocal microscopy images from 4 independent experiments with
812 replicates, showing pneumococcal (green) association with the epithelium (red, surface
813 carbohydrates; nuclei blue) at 6hr post infection. Bottom: Representative transmission electron
814 microscopy images from 2 independent experiments, showing pneumococcal microinvasion
815 examples of each strain (arrows), enclosed within a vacuole after 4hr infection. (B) Representative
816 confocal microscopy images from 4 independent experiments with replicates, showing
817 pneumococcal (green) interactions with junctional proteins (red) of β catenin. Colocalization of red
818 and green appears yellow. Nuclei (blue). (C) Integrated intensity of β catenin in pneumococcal
819 negative (not pneumococcal associated) or positive (pneumococcal associated) cells. Non infected
820 v pneumococcal negative cells **** p <0.0001 (NI v Δ*proABC/piaA*), ** p = 0.0026 (NI v Δ*fhs/piaA*);
821 non-infected v pneumococcal positive cells; **** p <0.0001 (NI v Δ*proABC/piaA* and NI v Δ*fhs/piaA*);
822 Kruskal-Wallis, n = 4 independent experiments. (D) Transepithelial electrical resistance (TEER) was
823 recorded pre- and post- 6hr infection to assess barrier integrity. N = 3 independent experiments with
824 replicates. Average TEER pre-infection was 466Ω.cm^2 (430-484 Ω.cm^2, p = 0.1458 ANOVA) and
825 average TEER post-infection was 545Ω.cm^2 (527-567 Ω.cm^2. p = 0.04744 ANOVA). Change in
826 TEER comparing non-infected cells to infected cells p = 0.6592, Kruskal-Wallis. Error bars represent
827 SEM.

828

829 **Fig 3. Pneumococcal – epithelial interactions with primary human epithelial cells.** Cells were
830 cultured at ALI and infected with pneumococcal strains for 6hrs. (A) Representative scanning
831 electron microscopy images from 2 independent experiments, showing the surface of the epithelium.
832 Representative examples of differentiated epithelia (basal cells, Clara cells, goblet cells, ciliated
833 cells) are shown in yellow text. Colonising pneumococci are highlighted by arrows. Representative
834 confocal microscopy images from 4 independent experiments with replicates for (B) Ciliated cells
835 (acetylated tubulin, red), (C) Goblet cells (mucin5ac, red, (arrows indicate co-localisation of
836 mucin5ac with pneumococci)), (D) Clara cells (uteroglobin, red) after 6hr infection. Pneumococci
837 (green), nuclei (DAPI, blue), colocalization of red and green appears as yellow. (E) Integrated
838 intensity of acetylated tubulin and Muc5ac in pneumococcal negative or positive cells from two or

839 more images. Acetylated tubulin, neg p = 0.2677, pos p = 0.017; Mucin5ac, neg p = 0.6852, pos p =
840 0.8510, ANOVA. N = 3 or 4 independent experiments. (F) Integrated intensity of uteroglobin
841 normalised to non-infected cells (left, p = 0.0115 non-infected v infected, Kruskal-Wallis) and
842 percentage of Clara positive cells following infection (right, p = 0.0003 non-infected v strains, p =
843 0.0036 6B v mutant strains, Kruskal-Wallis). N = 3 independent experiments.

844

845 **Fig 4**. **Strain association, microinvasion and transmigration of Detroit 562 cells.** Cells were
846 infected with *S. pneumoniae* for three hours and CFU counts recorded. (A) Representative confocal
847 microscopy images from 6 independent experiments with replicates, showing pneumococcal (green)
848 interactions with surface carbohydrates (red). (B) Association of pneumococcal strains to epithelial
849 cells. p = 0.0009 (Kruskal-Wallis), n = 6 with replicates. (C) Internalisation of strains into cells,
850 following a gentamicin protection assay. p = 0.0219 (Kruskal-Wallis) N = 6 with replicates. (D)
851 Microinvasive index is defined as the percentage of internalised bacteria over all associated bacteria.
852 p = 0.071 (Kruskal-Wallis) N = 6 with replicates. (E) Pneumococcal viability inside epithelial cells
853 following a gentamicin protection assay. n = 3 or 4 independent experiments with replicates. Counts
854 were normalised to microinvasion counts for each strain after 3 hours infection and compared to 6B
855 WT; +1hr p = 0.6517, +2hr p = 0.1377, +3hr p = 0.1183 (ANOVA). (F) Transmigration of
856 pneumococcal strains across confluent monolayers on transwell inserts. CFUs were recorded from
857 the basal chamber. N = 6 independent experiments with replicates. p < 0.001 (Kruskal-Wallis). (G)
858 Epithelial cell permeability was assessed via leak to 4kDa FITC-Dextran into the basal chamber. N
859 = 4 with replicates. p <0.0001 compared to non-infected cells, and p = 0.0689 between 6B WT and
860 mutant strains (Kruskal-Wallis). (H) Representative confocal microscopy images from 6 independent
861 experiments with replicates, showing pneumococcal (green) interactions with β catenin (red).
862 Nuclear DAPI stain (blue). (I) Image quantification of integrated intensity of β catenin normalised to
863 non-infected cells, following infection with the different strains. N = 5 independent experiments. Non
864 infected v pneumococcal negative cells **** p <0.0001 (NI v Δ*fhs/piaA*); non-infected v
865 pneumococcal positive cells; **** p <0.0001 (NI v 6B), * p = 0.0183 (NI v Δ*proABC/piaA*), * p = 0.0149
866 (NI v Δ*fhs/piaA*); Kruskal-Wallis.

867

868 **Fig 5. Detroit 562 cell transcriptomic responses to pneumococcal strains.** Epithelial cells were
869 infected for four hours with pneumococcal strains and RNA extracted and processed for RNAseq.
870 6B n = 11, PP n = 17, FP n = 14, non-infected n = 12, from 6 independent experiments. (A) All
871 significantly log2 fold change upregulated genes according to strain compared to non-infected cells.
872 Significance was defined as DEGs with a log2 fold change (logFC) of > 1.5 and false discovery rate
873 (FDR) of < 0.05. (B) Comparison of the top 20 most upregulated genes for each strain, compared to
874 non-infected cells. Upstream regulator analysis for (C) transcription factors and (D) kinases.

875

876 **Fig 6. Effects of pneumococcal infection on caspase activity in Detroit 562 cells.** Caspase
877 activity was assessed by luminescence, following infection with pneumococcal strains for 6 hours.
878 (A) Caspase 3/7 activity was determined following incubation with the specific inhibitor Z-VAD-FMK.
879 N = 4 with replicates. In comparison to non-infected cells, caspase 3/7 p = 0.0022; caspase 3/7 + Z-
880 VAD-FMK inhibitor p = 0.0005. In comparison to 6B WT, caspase 3/7 p = 0.0215; caspase 3/7 + Z-
881 VAD-FMK inhibitor p = 0.0012 (Kruskal-Wallis). (B) Caspase 1 activity was determined following
882 incubation with the specific inhibitor YVAD-CHO. Negative signals indicate caspase activity other
883 than caspase 1. N = 6 with replicates. In comparison to non-infected cells, p = 0.39; caspase+YVAD-
884 CHO inhibitor p = 0.3604 and, in comparison to 6B WT, p = 0.6226; caspase+YVAD-CHO inhibitor
885 p = 0.5386 (Kruskal-Wallis). (C) Caspase 8 activity was assessed following infection with
886 pneumococcal strains. N = 3 with replicates. In comparison to non-infected cells, p = 0.0015
887 (ANOVA) and, in comparison to 6B WT, p = 0.0172 (ANOVA).

888

889 **Fig 7. Hydrogen peroxide secretion and pneumolysin activity from pneumococcal strains in**
890 **the absence and presence of Detroit 562 cells.** A) Fold change of hydrogen peroxide production
891 from the mutants compared to WT, normalised to the CFU counts. 3hr p = 0.0087 (ANOVA), 6hr p
892 = 0.0209 (Kruskal-Wallis). B) Fold change of hydrogen peroxide production from the mutants
893 compared to WT, normalised to the CFU counts, following infection of Detroit 562 cells. Media was

894 replaced after 1hr infection and cells incubated for a further 5hrs. N = 3 independent experiments
895 with replicates. Compared to 6B WT, $p = 0.0034$ (ANOVA). C) Pneumolysin activity was assessed
896 using a red blood cell lysis assay. Strains were incubated with red blood cells for 30 minutes and
897 absorbance measured. N = 4 experiments with replicates. Pneumococcal strain haemolytic activity
898 is calculated in comparison to 100% lysis by 0.0625% saponin. $p < 0.0001$ compared to 6B WT
899 (ANOVA).

Table 1. Differentially expressed pathways from single isogenic mutants in human serum compared to WT.

Pathway	GeneRatio	P-adjust	qvalue
Δ*fhs* vs. WT			
Fatty acid metabolism/biosynthesis	10/57	1.08E-09	6.49E-10
Biosynthesis of secondary metabolites	26/57	2.09E-04	1.26E-04
Purine metabolism	10/57	1.34E-03	8.06E-04
Quorum sensing	11/57	3.20E-03	1.92E-03
Pantothenate and CoA biosynthesis	5/57	3.59E-03	2.16E-03
beta-Lactam resistance	5/57	7.59E-03	4.57E-03
Propanoate metabolism	4/57	1.51E-02	9.09E-03
2-Oxocarboxylic acid metabolism	4/57	1.51E-02	9.09E-03
Metabolic pathways	40/57	1.94E-02	1.16E-02
Amino sugar and nucleotide sugar metabolism	7/57	4.22E-02	2.54E-02
Pyruvate metabolism	5/57	4.31E-02	2.59E-02
Δ*proABC* vs. WT			
Fatty acid metabolism/biosynthesis	10/71	1.17E-08	8.94E-09
Galactose metabolism	12/71	1.25E-04	2.47E-08
Phosphotransferase system (PTS)	13/71	2.54E-03	1.93E-03
Amino sugar and nucleotide sugar metabolism	9/71	2.89E-02	2.20E-02

Figure 1. Pneumococcal – epithelial interactions in the EHPC model

A

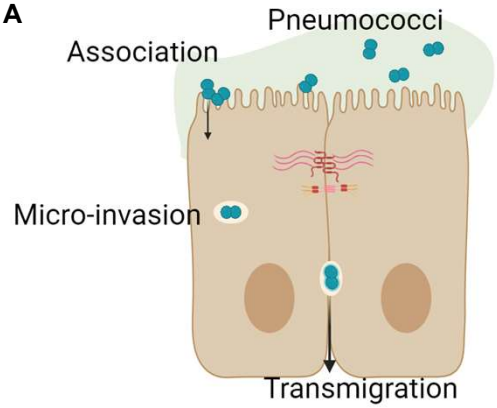

B

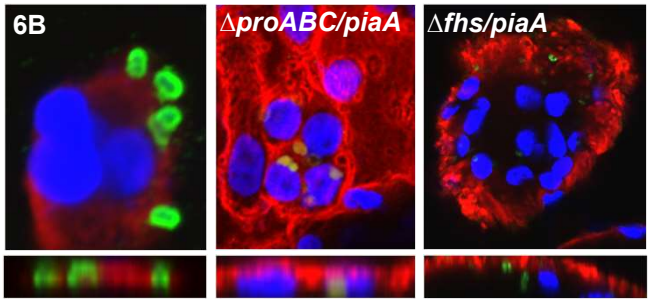

C

	Day 6 post-challenge	
	Association (%)	**Micro-invasion (%)**
6B	87.8 (n11, 43spn)	12.2 (n11, 6spn)
Δ*proABC/piaA*	59.3 (n11, 16spn)	40.7 (n11, 11spn)
Δ*fhs/piaA*	48.7 (n5, 57spn)	51.3 (n5, 60spn)

Figure 2. Impact of pneumococcal infection on NHBE-A cell junctional protein expression and barrier integrity.

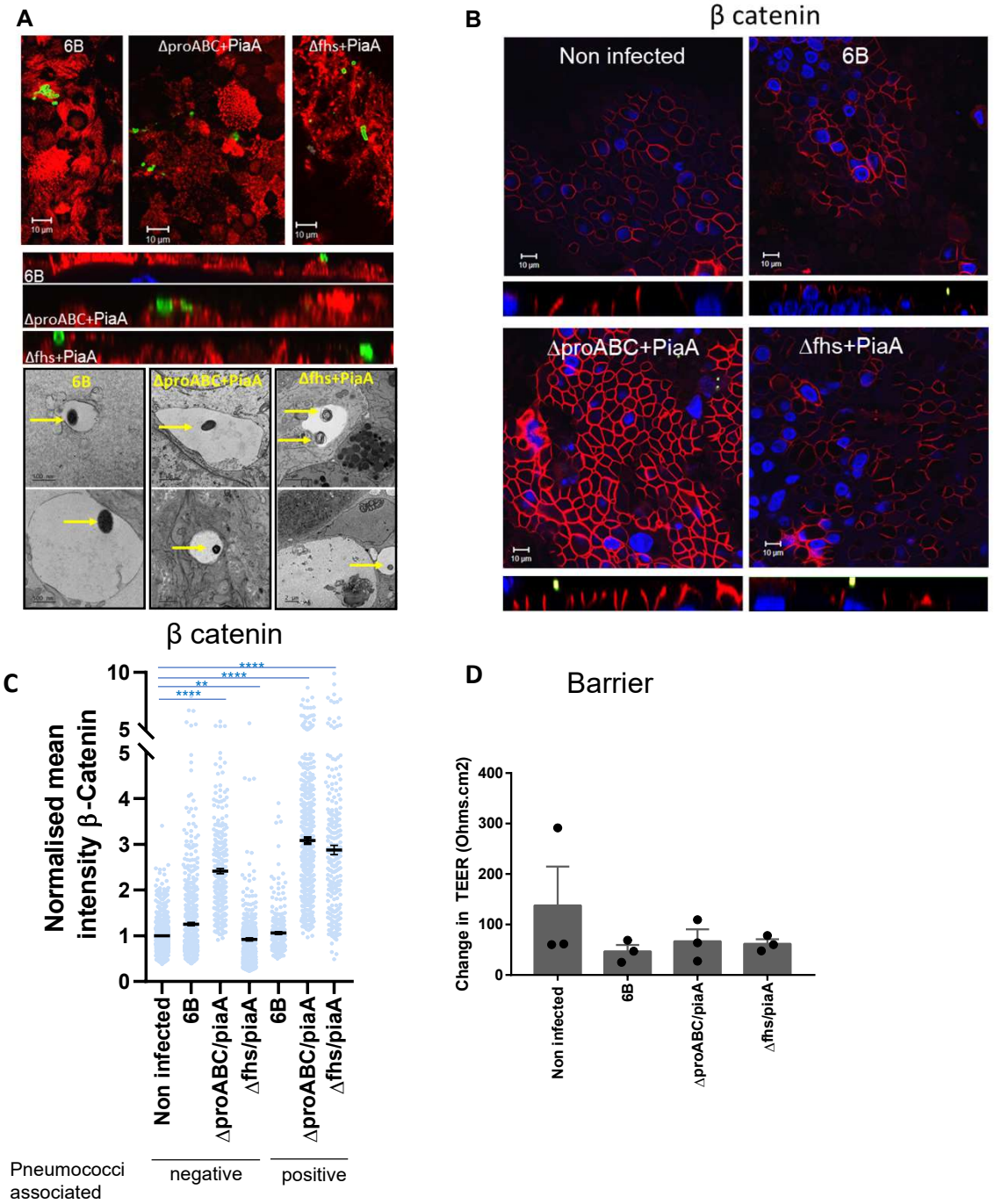

Figure 3. Pneumococcal – epithelial interactions with primary human epithelial cells.

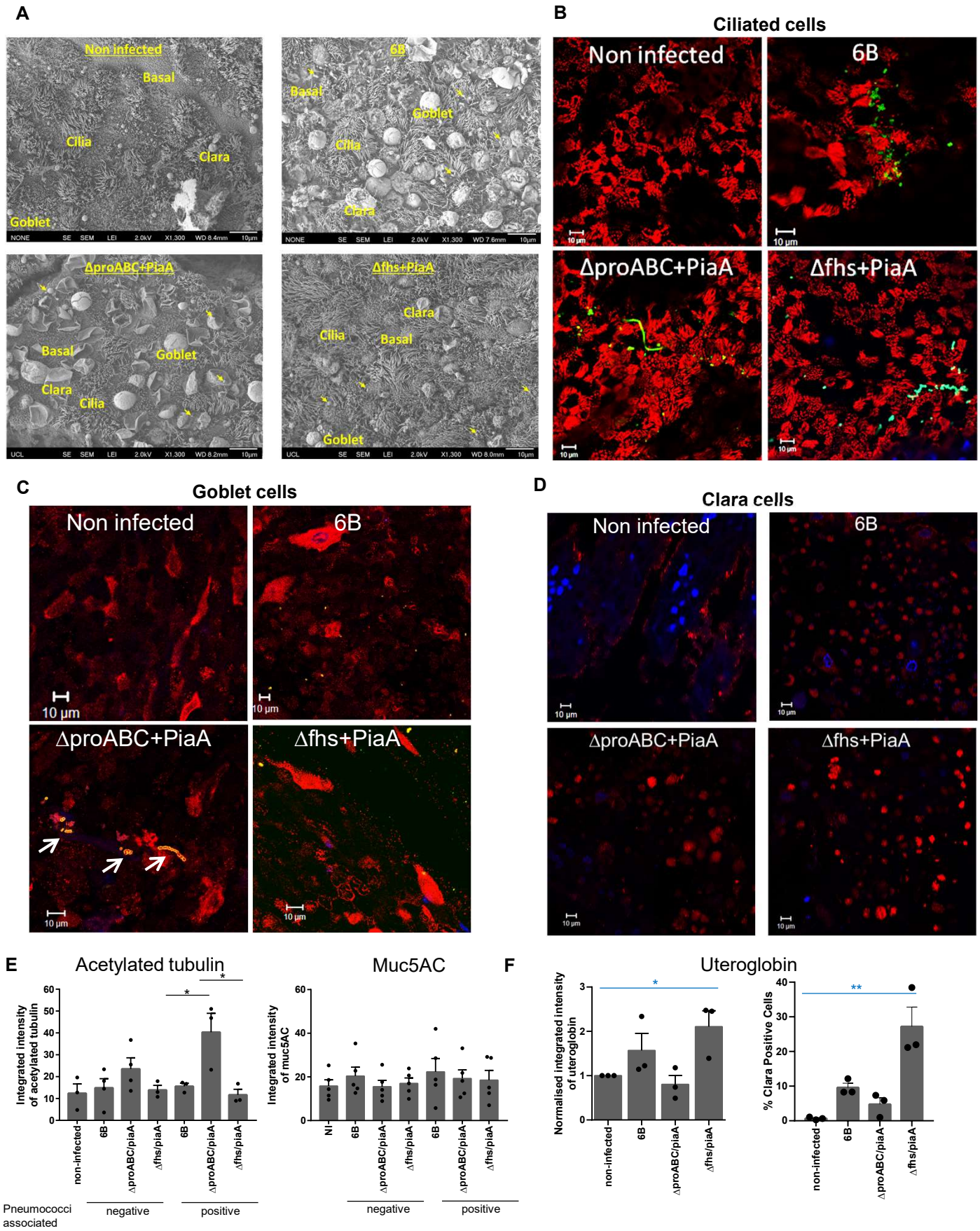

Figure 4. Strain association, microinvasion and transmigration of Detroit 562 cells.

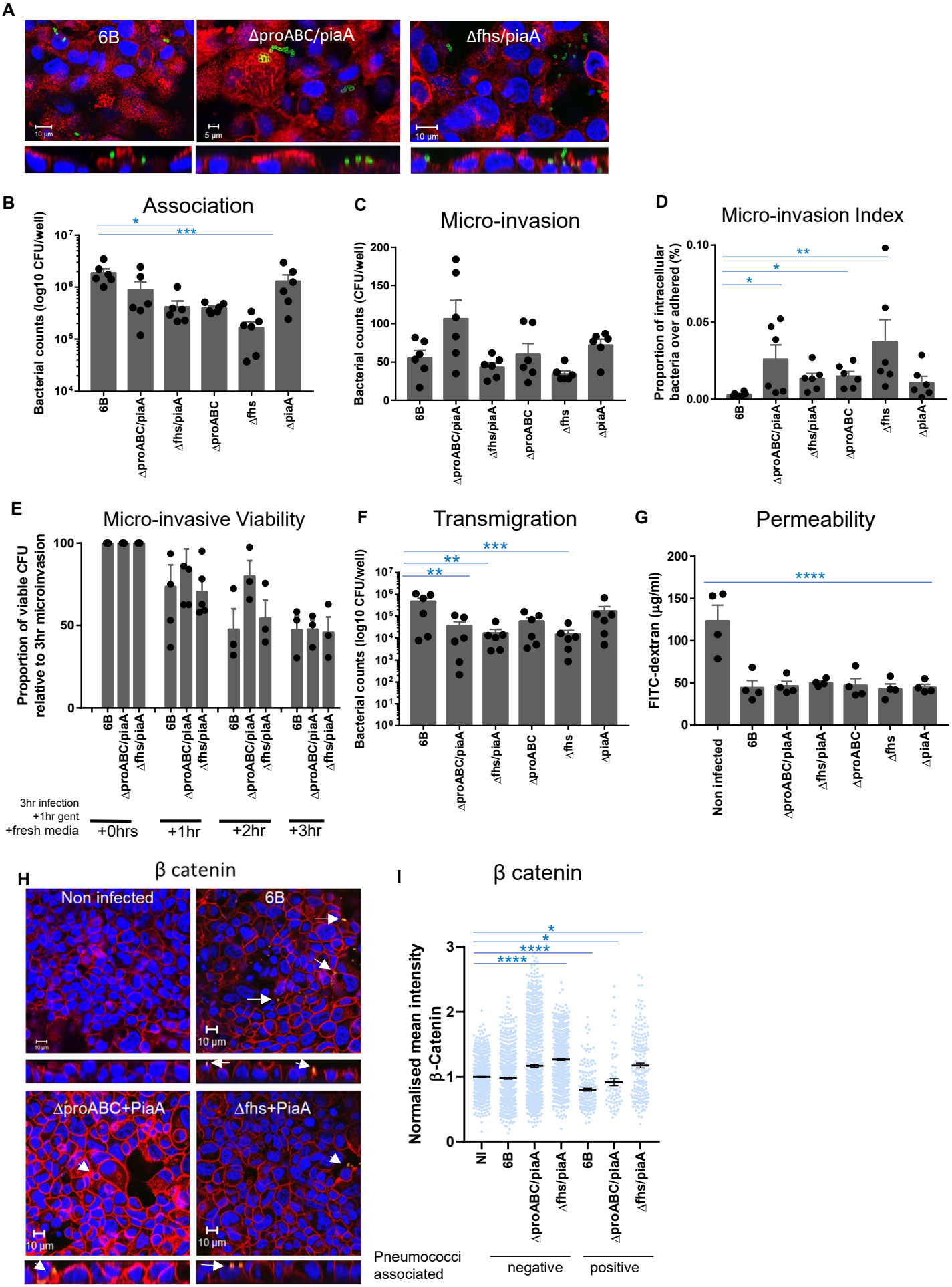

Figure 5. Detroit 562 cell transcriptomic responses to pneumococcal strains.

A

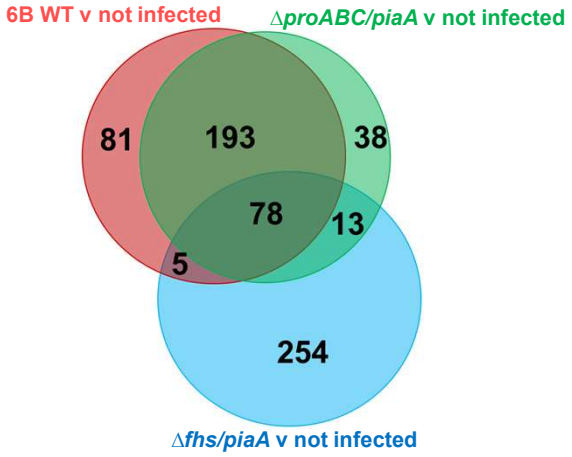

B

log2foldchange	6B	ΔproABC/piaA	Δfhs/piaA
Upregulated genes			
AC256236.1	32.9	25.5	0.0
AC022149.1	30.2	27.6	0.0
Z84488.2	29.1	21.6	0.0
MUC21	25.8	29.0	0.0
VASN	20.9	0.0	0.0
BRD2	18.4	24.7	0.0
AC012254.2	18.2	13.8	0.0
CTAGE4	18.1	0.0	0.0
MICE	17.1	20.3	0.0
AC107075.1	10.1	0.0	0.0
CSNK2B	0.0	20.2	0.0
MTRNR2L6	0.0	19.4	15.8
LSM2	0.0	17.1	0.0
ALOX5	0.0	0.0	6.9
AC006064.6	0.0	0.0	3.4
TAP2	0.0	0.0	3.2
CYP1A1	0.0	0.0	1.7
FOSB	0.0	0.0	1.4
IL1B	0.0	0.0	1.3
CXCL8	0.0	0.0	1.1
CXCL2	0.0	0.0	1.1
CYP1B1	0.0	0.0	1.0

C

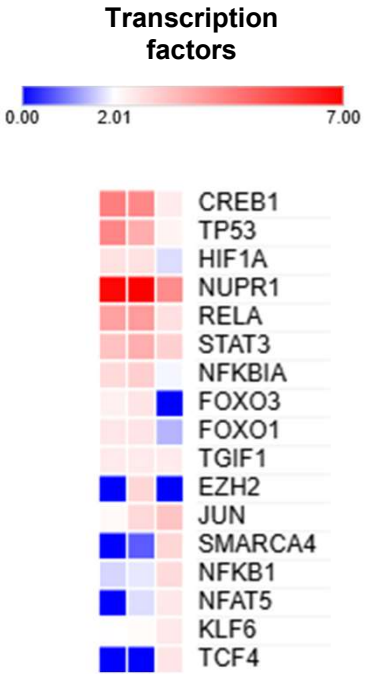

D

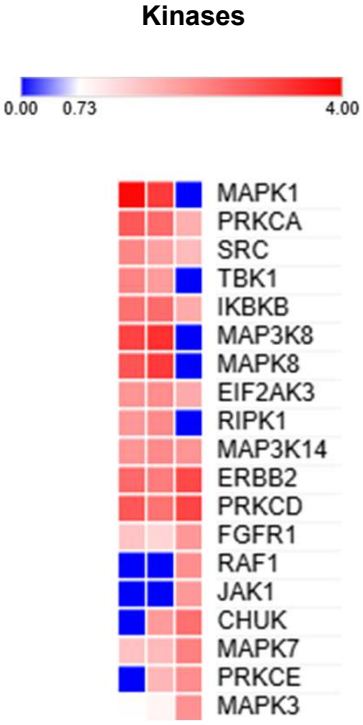

Figure 6. Effects of pneumococcal infection on caspase activity in Detroit 562 cells.

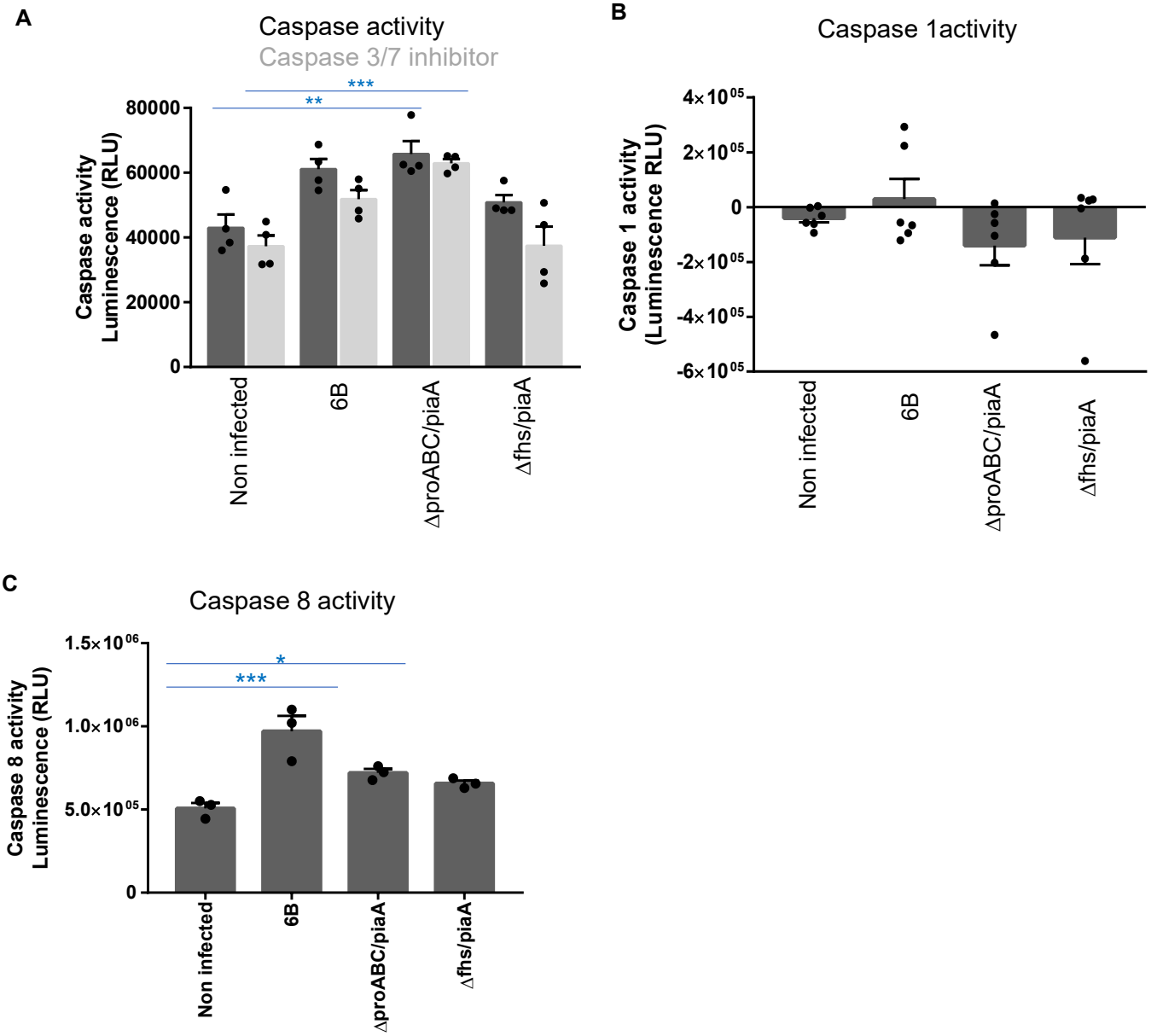

Figure 7. Hydrogen peroxide secretion and pneumolysin activity from pneumococcal strains in the absence and presence of Detroit 562 cells.

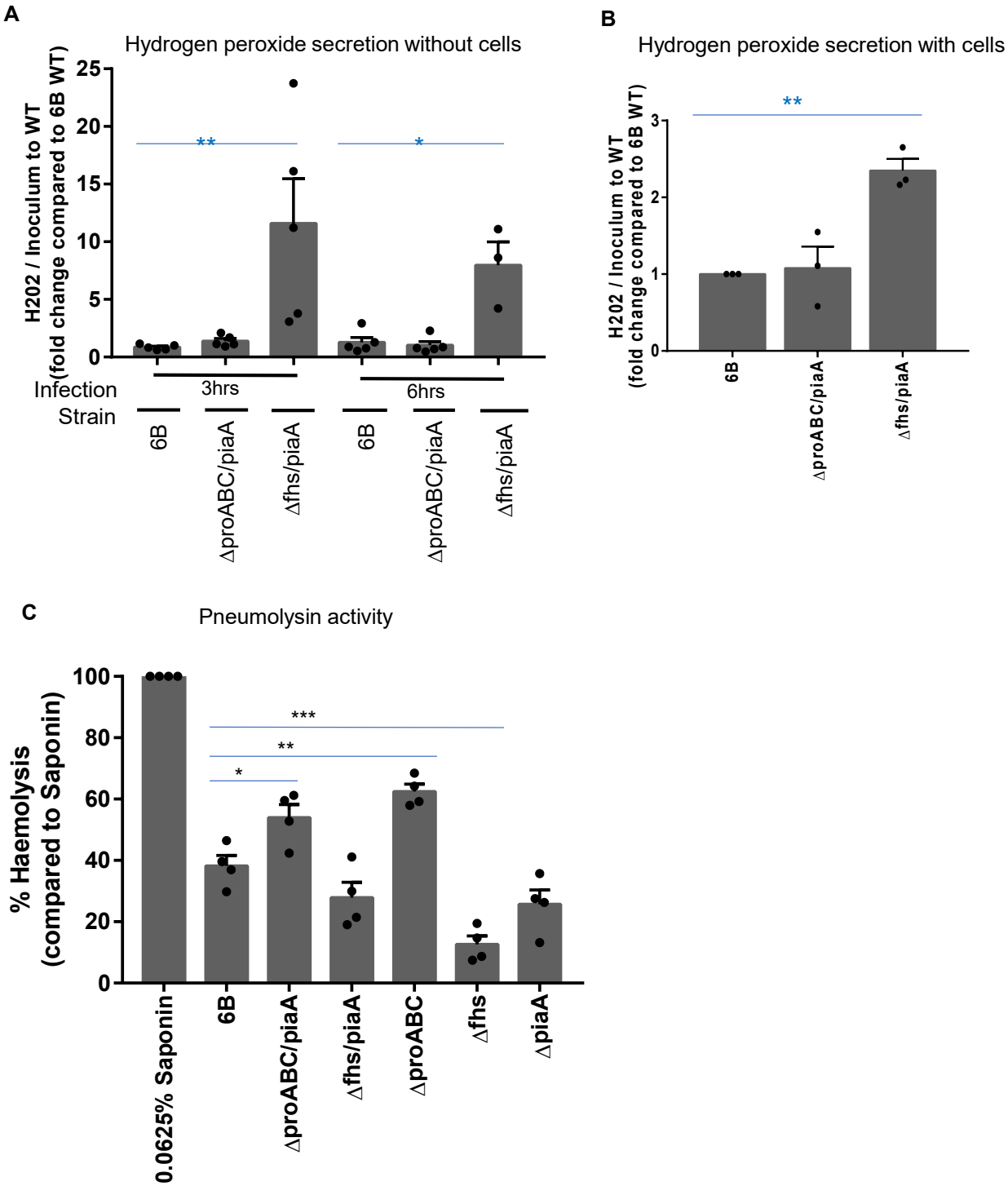
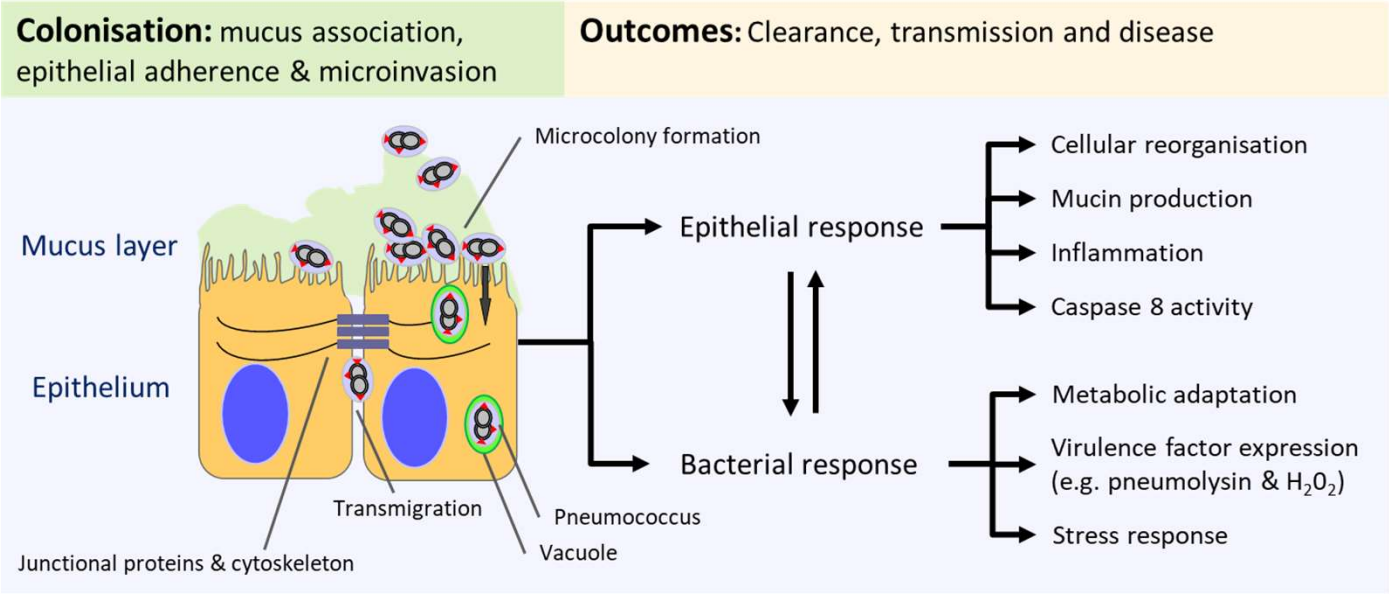
Graphical abstract